Atomistic simulations on the relationship between solid-phase epitaxial recrystallization and self-diffusion in amorphous silicon

Posselt, M.; Bracht, H.; Radic, D.;

Originally published:

January 2022

Journal of Applied Physics 131(2022), 035102

DOI: https://doi.org/10.1063/5.0078015

Atomistic simulations on the relationship between solid-phase epitaxial recrystallization and self-diffusion in amorphous silicon

M. Posselt[1*], H. Bracht[2], and D. Radić[2]

[1]Helmholtz-Zentrum Dresden – Rossendorf, Institute of Ion Beam Physics and Materials Research, 01328 Dresden, Germany
[2]University of Münster, Institute of Materials Physics, 48149 Münster, Germany

ABSTRACT

Recent experimental results on self-diffusion (SD) in amorphous silicon (a-Si) [J. Kirschbaum *et al.* Phys. Rev. Lett. **120,** 225902 (2018)] indicate that the atomic mechanism of this process is akin to that of solid-phase epitaxial recrystallization (SPER). In the present work, this relationship is investigated using classical molecular dynamics (MD) simulations with selected interatomic potentials. At the beginning an overview on the status of the present knowledge on SPER and SD is given. Then, it is shown that the Stillinger-Weber(SW)-type and Tersoff(T)-type potentials considered yield structural data of a-Si which are in rather good agreement with measurements. On the other hand, deviations are found for thermal properties. The results of partially extremely long MD calculations of SPER and SD yield that both processes can be described by a simple Arrhenius relation and that the activation enthalpies of SPER and SD are rather equal, which is in qualitative agreement with experiments. Obviously, the simulated atomic-level processes are very similar. However, for the known SW- and T-type interatomic potentials a quantitative agreement with SPER and SD measurements cannot be found. This work demonstrates that significant improvements can be achieved, if SW-type potentials with an increased value of the three-body parameter are used.

* Corresponding author,
Address: Helmholtz-Zentrum Dresden - Rossendorf, Bautzner Landstraße 400,
01328 Dresden, Germany
Electronic address: m.posselt@hzdr.de
Phone: +49 351 260 3279
Fax: +49 351 260 3285

I. INTRODUCTION

Amorphous silicon (a-Si) plays an important role in many applications. In nanoelectronic technology dopant atoms such as boron, phosphorus, or arsenic are introduced into the basic single-crystalline silicon (c-Si) material by ion implantation. Ultra-shallow p/n junctions with high dopant concentrations are accomplished by high ion fluences which often leads to the amorphization of c-Si. In order to realize shallow dopant profiles, c-Si may be also pre-amorphized by Ge or Si implants in order to minimize channeling effects during the implantation of dopants and to avoid the interaction of dopants with typical irradiation defects in c-Si such as self-interstitials and vacancies (see e.g. Refs. 1 and 2). In a post-implantation thermal treatment solid-phase epitaxial recrystallization of the amorphous layers is carried out and the dopant atoms are electrically activated. Furthermore, a-Si films are the basic material in display technologies [3], for solar panels [4], and are e.g. under discussion as alternative high capacity electrode material in Li ion batteries [5]. In these cases the amorphous films are prepared using a variety of methods such as plasma-enhanced chemical vapour deposition, chemical vapour deposition, sputter deposition, thermal evaporation, and picosecond or nanosecond laser melting followed by rapid quenching. Depending on the deposition process the properties of the films can vary strongly. In the present work compact a-Si without any foreign atoms and voids is considered. The structural, thermal and kinetic properties of this material are still not fully understood. Atomic-level calculations can contribute to get more insights. Recent experimental investigations [6] demonstrated that the activation enthalpy of self-diffusion (SD) in a-Si is very similar to that of solid-phase epitaxial recrystallization (SPER). This confirms earlier assumptions that both processes might be governed by the same mechanisms. In the present work the velocity of SPER and the SD coefficient are determined by classical Molecular Dynamics (MD) simulations. The focus is on the search for interatomic potentials enabling a satisfactory simulation of both effects. Due to the computational effort required for obtaining results which are comparable with measured data, more sophisticated methods such as tight-binding and first-principle calculations cannot be employed here.

The work is organized as follows: At first a review of recent and previous findings on SPER and SD is given. Then, the computational preparation of a-Si is presented for the different interatomic potentials, followed by the discussion of the obtained structural and thermal properties. The next two parts deal with MD simulation of SPER and SD. The data obtained by using several interatomic potential are compared with the available experimental data. Finally, the results for SPER and SD are compared for the respective potentials and the similarities and differences are discussed.

II. SUMMARY OF THE STATUS OF RESEARCH

A. Solid-Phase Epitaxial Recrystallization (SPER)

Since the seventies of the last century SPER of a-Si layers on c-Si substrates has been studied intensively. Several reviews on experimental methods and obtained results are available (see Refs. 7 and 8). In the following the focus is on SPER of pure a-Si layers at

normal pressure. An important result of the experimental investigations is the fact that within a wide temperature range the velocity of SPER can be described by a single Arrhenius-type relation. Activation enthalpies between 2.35 [9] and 2.85 eV [10] were obtained. For the broadest region of temperatures, from 470°C up to the melting point, Olson and Roth [7] found an activation enthalpy of about 2.75 eV. In this case amorphization was performed by arsenic implantation at moderate fluence. Comprehensive investigations of SPER of thicker a-Si layers formed by self-ion implantation led to an activation enthalpy of 2.70 eV [11]. Most experimental investigations considered SPER of a-Si formed by ion implantation. However, also SPER of a-Si deposited on c-Si was studied and nearly the same activation enthalpy was measured [7]. By comparing SPER of as-implanted a-Si with that of structurally relaxed (by gentle thermal annealing after implantation) a-Si Lu *et al.* [12] and Roorda *et al.* [13] showed that SPER is not affected significantly by this relaxation. It was also found that hydrogen contamination during annealing does not influence the value of the activation enthalpy of SPER [11,14] but leads to the reduction of the pre-factor in the Arrhenius-type relation. Investigations of SPER of amorphous Ge demonstrated that this process may be explained by bond rearrangements with minimal atomic displacements at and near the interface [15]. SPER of a-Si should occur in the same manner. The study of the dependence of the SPER velocity on the crystallographic orientation of the single-crystalline substrate led to the result that the activation enthalpy is nearly independent of the substrate orientation whereas the pre-factor strongly varies [9]. Amongst the main crystallographic directions, SPER into <100> is faster than SPER into <110> which is faster than SPER into <111>. In the latter case stacking fault and twin formation often prevent a defect-free recrystallization.

Already in the early stage of research on SPER, atomic models of the a-c interface were developed, in particular for a-Si on (111) and (100) c-Si [16,17]. It was found that the {111} interface should be planar, whereas the {100} interface may show a certain degree of roughness. This was also confirmed within the framework of the widely accepted atomic-level model of Csepregi *et al.* [9] which is based on the assumption that an atom initially belonging to a-Si becomes part of c-Si if it has at least two nearest neighbors already belonging to c-Si. In this manner it can be clearly explained why the SPER on a (100) substrate is fastest, and why SPER on a (111) substrate is slowest. [9,18]. Furthermore, within this qualitative model SPER proceeds generally on {111} terraces via adding of atoms from a-Si on {110} ledges which are situated at both sides of kinks [19-21]. Features of the (100) interface were also studied by tight-binding calculations [22].

In the last three decades several authors studied SPER by kinetic Monte-Carlo simulations (KMC) and MD. Non-lattice KMC [23,24] are based on the assumption that a-Si consists of a continuum of pairs of vacancies (V) and self-interstitials (I), and that the I-V recombination barrier depends on whether the neighbors are within a- or c-Si . Data from measurements of crystallization kinetics are used for the barrier height in the two limiting cases where (i) the IV pair is within bulk a-Si (5 eV, random nucleation) and (ii) at the planar a-c interface (2.7 eV, SPER), whereas the value for the IV pair in c-Si (0.43 eV) was obtained by MD simulation [23]. This simple and elegant method allows the study of recrystallization of a-Si and investigations of the formation and evolution of extended defects existing in c-Si after incomplete SPER. The lattice KMC of Martin-Bragado *et al.* [25-27] start from the model of Csepregi *et al.* [9] mentioned above and the experimental orientation-dependent SPER rates.

These authors performed studies on details of SPER such as orientation and stress dependence, and interface topology.

MD simulation using interatomic potentials [28-34,36-39] is a more fundamental method to treat SPER since it does not require inputs directly obtained from measurements. However, numerous publications showed that the choice of the interatomic potential has a decisive influence on the results. This concerns particularly the value of the SPER velocity in dependence on temperature which can be directly compared with the measured data. Krzeminski *et al.* [32-34 performed a comprehensive comparison of own results obtained by different potentials with corresponding literature data. A satisfactory agreement with (the high-temperature extrapolation of the fit to) experimental data was only obtained for the Tersoff potential [35]. On the other hand, the SPER velocity calculated (for zero pressure) by Shanavas *et al.* [36] using the Tersoff potential is smaller than that of Krzeminski *et al.* [32-34]. In several SPER studies by MD the qualitative models of Csepregi *et al.* [9] were confirmed and also previously predicted defects [37] at the (100) a-c interface could be identified [38]. However the measured difference between SPER velocities into <100>, <110>, and <111> directions could not be reproduced quantitatively [33,34]. Not only the MD simulations of SPER of a-Si but also those of SPER of a-Ge [40] revealed that local bond switching and rearrangement processes are responsible for the transfer of atoms from the amorphous to the crystalline state.

B. Self-Diffusion (SD)

Direct measurements of SD in a-Si have been performed only recently [41,6]. This was due to the difficulty to suppress two processes competing with SD: (i) SPER since the a-Si layer is commonly prepared on respective c-Si substrates by deposition or self-ion implantation and (ii) random nucleation of the crystalline phase within a-Si. A further reason was the requirement for very precise analytical techniques based on the use of isotopically modified multilayers and the corresponding depth profiling techniques.

In the study of Strauß *et al.* [41] an amorphous $^{29}Si/^{nat}Si$ isotope multilayer structure was prepared by magnetron sputtering on a crystalline Si wafer and the depth profiling was performed by neutron reflectometry and secondary ion mass spectrometry (SIMS). These authors report an activation enthalpy of 4.4 eV for SD in the temperature range between 550 and 700°C. The investigations of Kirschbaum *et al*. [6] used an epitaxially grown $^{nat}Si/^{28}Si$ stack on top of a silicon-on-insulator (SOI) substrate that was amorphized by Si ion-implantation. SD studies were performed at temperatures between 460 to 600°C and SIMS was applied to measure diffusion broadening of the isotope layers. An activation enthalpy of 2.70 eV was found. Considering the velocity of SPER reported in the literature [7,8], the amorphous layer prepared by Strauß *et al.* [41] should be fully recrystallized during their diffusion anneals. Therefore, it is very likely that SPER in the samples of Strauß *et al*. was suppressed by the existing high level of carbon contamination [41].This questions the high activation enthalpy of SD reported by Straus *et al*. so that the value of Kirschbaum *et al.* [6] should be the correct one. The results obtained in Ref. 6 also indicate that structural relaxation of as-implanted a-Si is an initial (i.e. short-time) process characterized by local and short-range ordering, as

reported by Roorda *et al.* [42], and thus does not significantly affect SD. The discussion in Ref. 6 led to the conclusion that SD in a-Si should be mediated by local bond rearrangements. As mentioned above, this kind of processes was also assumed to be responsible for SPER of amorphous Ge [15,40]. This may explain the fact that the activation enthalpies of SD and SPER are nearly equal.

Numerous investigations were performed in the past 30 years to study the interdiffusion of a-Si/a-Ge multilayers [43-51] and diffusion of foreign atoms in a-Si [52-54]. In some cases these investigations allow an estimation of the SD coefficient in a-Si. In a recent paper, Noah *et al.* [43] obtained this quantity by investigation of the interdiffusion in an a-Si/a-$Si_{1-x}Ge_x$ ($0 \le x \le 0.48$ at%) multilayer structure that was prepared by evaporation of Si and Ge in ultra-high vacuum, on a (100)-oriented Si substrate covered with Si_3N_4. The deposition on top of the Si_3N_4 layer avoids direct contact of the amorphous Si/SiGe multilayer structure with the crystalline substrate and thus impedes SPER during diffusion annealing. Auger electron spectroscopy sputter-depth profiling was employed for analysis. In the temperature range between 440°C and 460°C Noah *et al.* [43] estimated an activation enthalpy of 2.1 eV for SD in pure a-Si. This value is closer to that of Kirschbaum *et al*. [6] than to that of Strauß *et al.* [41]. Also the measured SD coefficients fit well to the data of Ref. 6 while they are much higher than those of Ref. 41. It is worth noting that at low concentrations the diffusion of H in a-Si can be characterized by an activation enthalpy of 2.7 eV [52], and for B diffusion in a-Si a similar value was found (3.0 eV, [54]). The migration of dangling and floating [55] bonds as well as bond rearrangement were proposed [54] as basic atomic mechanisms and it was concluded that the rate limiting process should be the same as in SPER.

The few theoretical investigations on SD in a-Si hitherto performed led to strongly different results. Song *et al.* [56] used a Stillinger-Weber interatomic potential [57] with an increased three-body parameter ($\lambda = 31.5$), together with the nudged elastic band method in combination with the activation-relaxation technique [58,59], in order to determine the energy barriers between the plethora of states possible in a defect-free (fourfold coordinated) a-Si structure. They found an average barrier height for SD of about 3 eV and the bond exchange proposed by Wooten *et al.* [60] as the most important mechanism for non-defect based diffusion events. Using the mean attempt frequency of 18.8 ps^{-1} obtained in Ref. [56] leads to a pre-exponential factor of 7.0×10^{-3} cm^2s^{-1} and, finally, to a SD coefficient of about 2.8×10^{-17} cm^2s^{-1} at 1050 K (777°C). Sastry *et al.* [61] used MD simulations with the original Stillinger-Weber potential [57] and obtained a value of 6.4×10^{-8} cm^2s^{-1} at a temperature of 1060 K (787 °C). A similarly high (and unrealistic) SD coefficient was found by tight-binding MD calculations of Santos *et al.* [62]. These authors considered both defect-free a-Si prepared by the WWW algorithm [60] and a sample prepared by quenching from the liquid phase with 20% fivefold-coordinated atoms. In the first and the second case the obtained self-diffusion coefficients were $D=4.2 \times 10^{-4} \exp(-0.95\ eV/k_BT)$ cm^2s^{-1} and $D=2.8 \times 10^{-4} \exp(-0.86\ eV/k_BT)$ cm^2s^{-1}, respectively. Obviously, the initial miscoordination does not significantly influence the results of these tight-binding MD simulations.

General theoretical investigations on the diffusion in simple, strongly disordered, amorphous model systems reveal that SD in these materials shows a nearly Arrhenian behavior [63,64]. This was explained by compensation between site and saddle disorder, i.e.,

between the statistical distribution of the energy differences between final and initial state and the distribution of the energy barriers.

III. PREPARATION OF AMORPHOUS SI AND ITS STRUCTURAL AND THERMAL PROPERTIES

Using MD simulations, a-Si is prepared in the present work by (i) melting of diamond-structure c-Si, (ii) equilibration of the melt for several 100 ps, (iii) cooling of the system to 300 K at a cooling rate of 0.1 K/ps, and (iv) equilibration at 300 K for some 100 ps. Also higher cooling rates were investigated and it was found that below 10 K/ps the characteristics of a-Si do not alter significantly. The calculation starts with a cubic supercell, with x-, y- and z-directions parallel to the [100], [010] and [001] axes, respectively. Three-dimensional periodic boundary conditions and the isobaric-isothermal ensemble (N,P,T with $P=0$) are considered. The simulation cell is coupled to a Berendsen thermostat and a Berendsen barostat [65]. In most of the calculations the simulation cell contains 1000 atoms, i.e. with the dimensions $5d\times5d\times5d$ where d is the lattice constant, but also a cube with 4096 atoms and the dimensions $8d\times8d\times8d$ is considered. In the following subsections more details concerning the preparation of a-Si performed in the present work by using different interatomic potentials are described, and the results on structural and thermal properties are discussed. The investigations are limited to Stillinger-Weber (SW)- and Tersoff (T)-type potentials since these were successfully applied in a plethora of publications on condensed phases of Si, Ge, and Si_xGe_{1-x}. In the last three decades a lot of interatomic potentials for Si were developed (see Refs. 66-79) but, unfortunately, all of them cannot be considered in this article. This is also due to the fact that SW- and T-type potentials allow rather efficient calculations which is very important for comprehensive computational tasks such as near-realistic MD simulation of SPER and SD. The time steps in MD simulations are 1 fs and 0.5 fs if SW- and T-type potentials are used, respectively.

A. Stillinger-Weber-type (SW) interatomic potentials

1. SW potential of Balamane et al. [80]

The potential is identical to the original SW potential [57] with the exception of the value of the energy scaling parameter ε that is set to 2.315 eV in order to reproduce the correct ground-state cohesive energy per atom (-4.63 eV) of c-Si. More details can be found in the Supplementary Material [81]. It was already mentioned by Stillinger and Weber [57] that direct freezing of liquid-Si (l-Si) by MD simulation does not lead to a-Si with realistic properties. On the other hand, l-Si can be well described using the SW potential. Also the application to c-Si yields satisfactory results in many cases. Luedtke and Landman [82] (see also Refs. 38 and 40) developed a procedure to prepare a realistic a-Si material. A very similar method is employed in this work: In the first simulation step liquid Si is produced by equilibrating the system at 2700 K. Then, the value of the three-body parameter of the SW potential is increased

by a factor of 1.5 (i.e. from $\lambda = 21$ to $\lambda = 31.5$), and a second equilibration is performed. In the next step the system is cooled down to 300 K. The increase of the three-body parameter leads to enhanced preference for the tetrahedral coordination. After cooling, at 300 K the three-body parameter λ is set back to 21 and the system is equilibrated once more for some 100 ps. In the following it will be shown that the simulation method described above yields a-Si with good structural and satisfactory thermal properties. Obviously, authors of some recent papers (see e.g. Ref. 83) did not know the relatively old work of Luedtke and Landman [82] and claimed that SW-type potentials are not able to generate realistic a-Si. It must be emphasized that the present computational method to produce a-Si does not correspond to a real cooling process. On the other hand, in experiments the metastable amorphous Si phase is not prepared by a quasi-equilibrium cooling from liquid Si, but by non-equilibrium methods such as self-ion implantation (see e.g. Refs. 84-91) various deposition methods (see e.g. Refs. 87 and 92-94), a rapid melt-quench procedure initiated by laser irradiation [87], and by mechanical indentation [83,95]. Furthermore, theoretical and experimental investigations (see e.g. Refs. 96-99) indicate that the difficulty to obtain a-Si using a quasi-equilibrium cooling may be also due to the existence of an intermediate high-density amorphous state so that a poly(a)morphic transformation between l-Si and a-Si may occur.

Results of the MD preparation of a-Si as outlined above are depicted in Fig. 1 and in Table I. Fig. 1 shows various properties: (i) pair correlation function. (ii) static structure factor, (iii) bond-angle distribution, and (iv) the distribution of the dihedral angle. Only the static structure factor, i.e. the Fourier transform of the pair correlation function, is directly accessible by measurements. Fig. 1 (b) shows a good agreement of the simulation result with experimental data for the static structure factor obtained by X-ray or neutron diffraction. Note that in experiments a-Si was prepared by different methods: (i) self-ion implantation and subsequent (gentle) annealing [90,91,100], and (ii) sputter deposition or e-beam evaporation, plus annealing [92,93]. Xie *et al.* [100] performed detailed X-ray measurements of the static structure factor for large and very large wavelengths. The inset of Fig. 1 (b) presents their data in comparison with the present MD results for the region around the first peak. The height of this peak (see Table I) is usually taken as a measure for the degree of structural ordering or relaxation of a-Si [101]. The comparison with the X-ray data for annealed a-Si with the results of a-Si prepared by MD demonstrates that the simulated a-Si is sufficiently relaxed. For a further test of the thermal stability, the MD system was reheated to 1100 K and cooled down to 300 K. The structural properties (at 300 K) obtained after this treatment are almost identical to those of the originally prepared a-Si. This demonstrates once again that the prepared a-Si exhibits a sufficient degree of relaxation and ordering. The bond-angle distribution [Fig. 1 (c)] shows a pronounced peak close to the tetrahedral angle that is characteristic for c-Si. In the present case a mean bond angle of 109.0° and a root mean square (*rms*) deviation of 10.7° is obtained. In order to determine the bond (and dihedral) angles a bond-cutoff of 2.95 Å is generally used. This value corresponds to a position at or close to the minimum between the first- and second-neighbor peaks in the pair correlation function. It is well known that a-Si exhibits a significant short-range order which can be also clearly seen in the present representations for pair correlation function and bond-angle distribution. Fig. 1 (d) depicts the distribution of the dihedral angle which is defined as the angle of rotation about a common bond of two tetrahedral units. In c-Si this distribution has delta-function-like peaks at 60 and

180°. Fig. 1 (d), but also Fig. 1 (a) demonstrates that in a-Si not only a short-range order similar to c-Si exists, but also an intermediate or medium-range order, i.e. and order beyond the first neighbor atoms. This order may be also characterized by the difference between maximum and minimum of the distribution depicted in Fig. 1 (d). In Ref. 83 intermediate range order was characterized experimentally by the ratio of the TA (transversal acoustic) and TO (transversal optic) peaks of Raman spectra and correlated to the inverse of the maximum of the dihedral angle distribution. A technique that can offer insight into medium-range order is fluctuation electron microscopy. This method uses transmission electron microscopy (TEM) and statistically evaluates intensity fluctuations of TEM images/diffraction patterns of amorphous materials [102].

Table I presents structural data at 300 K determined by present MD simulations: atomic density, relative density difference between a- and c-Si, mean values of the coordination number and of the bond angle (and its *rms* deviation), the heat of crystallization of a-Si, the height of the first peak in the representation of the static structure factor as well as the difference between the extrema in the distribution of the dihedral angle. For comparison, selected experimental data from literature are shown in Table II. An overall good agreement with measurements is found for the density, the bond-angle characteristics and the height of the first peak of the static structure factor. On the other hand, the calculated heat of crystallization is somewhat higher than the estimated experimental value. Furthermore, the experimental mean coordination number estimated from the Fourier transform of the measured static structure factor is slightly less than 4, in contrast to the present MD results. Table III summarizes theoretical results from literature. For a consistent comparison with Table I, Table III shows only theoretical data obtained by (a certain kind of) melting and subsequent cooling. MD using interatomic potentials, Tight-Binding-(TB) MD, Density-Functional-Theory (DFT) MD as well as combined methods were employed to obtain these data. Regardless a certain scattering, the numbers given in Table III are rather similar to the results of present calculations. In particular the coordination numbers are also above 4 in many cases. It should be noticed that in many theoretical investigations mentioned in Table III the experimental value for the density of a-Si (or of c-Si) is used to obtain the properties of a-Si at 300 K, whereas in the present work this density is obtained from MD simulations in the isobaric-isothermal ensemble (N, P, T with $P = 0$). Interestingly, in some of the papers listed in Table III the MD cell contains a much larger number of atoms than in the present work but the data are more or less consistent with the results shown in Table I.

Furthermore, melting of a-Si was studied. MD simulations were carried out using a N, P, H ensemble (with $P = 0$), where H is the total enthalpy. Heating is performed by the continuous but slow increase of the velocity of atoms and zero pressure is maintained using a Berendsen barostat [65]. This method yields only reliable results if the increase of the atomic velocities is sufficiently slow, in particular near the transition temperature [40]. More details can be found in the Supplementary Material [81]. The characteristics of the melting process depicted in Fig. 2 are typical for a first order phase transition. However, one has to keep in mind that this is a transition from metastable a-Si to a supercooled liquid phase. The melting point and the heat of melting are 1348 K and 0.12 eV, respectively, which is consistent with

Ref. 82. The first value is somewhat lower than the data obtained by electrical conductivity measurements (1460-1480 K [117]) and agrees with an estimation from the experimentally determined heat capacity (1315-1420 K [85]). Since a-Si is a metastable phase it is difficult to observe melting without the preceding formation of crystalline nuclei. In practice, this problem may be circumvented by ultra-short time melting, e.g. by laser irradiation. Present simulations are similar to this process. The calculated heat of melting is lower than that determined from heat capacity data (0.384-0.388 eV [118]). Like in the case of crystalline Si, Ge, and water, melting of a-Si leads to an anomalous increase of the density. The present simulations yield a density increase of about 9%.

2. SW potential of Vink et al. [103]

The parameters ε and λ of the original SW potential [57] were set to 1.64833 and 31.5 ($=1.5\lambda_0$ with $\lambda_0 = 21$), respectively, based on a fit to data obtained from investigations of a-Si by Raman spectroscopy. Without using the special procedure of Luedtke and Landman [82], melting of c-Si (at 2700 K) and direct cooling within the framework of the isobaric-isothermal ensemble provides a-Si with reasonable structural characteristics: (i) the static structure factor is in good agreement with measurements, (ii) the mean coordination number, and (iii) the mean bond angle and its *rms* deviation are consistent with literature data, see Tables I, II, and III. On the other hand, the atomic density is slightly higher than the experimental value and the heat of crystallization is wrong. The latter is due to the chosen value of ε. The calculated melting point of a-Si and the heat of melting are 2065 K and 0.17 eV, respectively, which differs from the experimental data. Furthermore, there is a density decrease upon melting which is in contrast to reality. Results similar to Figs. 1 and 2 can be found in the Supplementary Material [81]).

3. SW potential of Albenze et al. [104]

These authors also changed the potential parameters ε and λ (ε=1.5175 and $\lambda = 1.15\lambda_0$) in order to improve thermal and structural properties of a-Si. Melting of c-Si (at 2700 K) and direct cooling under the condition of the isobaric-isothermal ensemble leads to reasonable data for the static structure factor, the atomic density, the mean coordination number, the bond angle characteristics, the heat of crystallization, see Tables I, II, and III, and the melting temperature (1360 K). The calculated heat of melting (0.14 eV, with a density increase of 2.4%) is lower than the experimental value. Other relevant results are given in the Supplementary Material [81].

4. Modified SW potentials proposed in this work

The consideration of the SW-type potential of Balamane *et al.* [80] in Sec. III A 1 indicates that a suitable choice of the three-body parameter λ during cooling is important for getting realistic room-temperature characteristics, i.e. a significant short-range order, a dominating tetrahedral coordination, a density slightly lower than that of c-Si, etc. On the other hand, one may conclude from the results obtained by the SW-type potential of Vink *et al.* [103] in Sec. III A 2 that a permanently higher λ leads to an unrealistic melting behavior. Indeed, in present

studies it was found that using the parameters of Balamane *et al.* [80] but with λ above a value of $\lambda = 1.2\lambda_0$ does not give a first-order phase transition between a- and l-Si. However, such higher values of λ are important for MD simulation of SPER and SD, as it will be shown later. In order to describe the phase transition between a-Si and l-Si in cases of high λ values approximately, a temperature dependence of λ can be introduced using a step-like function near the melting point. Two cases are illustrated below:

$$\lambda(T) = \lambda_0 \left\{ 0.15 \left[1 - \tanh\left(\frac{T - 1500}{100} \right) \right] + 1 \right\} \qquad \begin{array}{l} T \to 0 : \lambda = 1.3\lambda_0 \\ T \to \infty : \lambda = \lambda_0 \end{array} \qquad (1)$$

and

$$\lambda(T) = \lambda_0 \left\{ 0.2 \left[1 - \tanh\left(\frac{T - 1400}{100} \right) \right] + 1 \right\} \qquad \begin{array}{l} T \to 0 : \lambda = 1.4\lambda_0 \\ T \to \infty : \lambda = \lambda_0 \end{array} \qquad (2)$$

where $\lambda_0 = 21$ is the value in the original SW potential which allows a satisfactory description of c- and l-Si. The first case is illustrated in Fig. 3 for cooling and melting. Because of the chosen functional form for $\lambda(T)$ the melting temperature (1565 K) is not far from the experimental value, whereas the heat of melting (0.14 eV) is too low, as in the case of the other SW-type potentials. The density increase during melting is about 10%. Fig. 3 also demonstrates that cooling and melting are reversible as in case of most of the other interatomic potentials studied in the present work. The potential of Eq. (2) leads to a melting temperature and a heat of melting of 1495 K and 0.12 eV, respectively. After cooling to 300 K and equilibration both modified potentials yield structural properties which are in satisfactory agreement with literature data, see Tables I, II, and III. However, the heat of crystallization is too high. More data can be found in the Supplementary Material [81].

One may argue that the use of a temperature-dependent parameter in the interatomic potential violates the concept of separation between mechanical and thermodynamic quantities in statistical physics. The latter quantities are generally related to the chosen ensemble and to averaging of data provided by the atomistic mechanics. The above objection is certainly true. Therefore, modification (1) and (2) may be considered purely empirical. On the other hand, instead of using a temperature-dependent parameter λ one could also introduce a suitable, temperature-dependent volume change within the framework of a $N, V(T), T$ ensemble in order to obtain a satisfactory description of the density of a-Si and of the a-l phase transition. For example, a $V(T)$ procedure was used in DFT-MD preparation of a-Si by cooling from the melt by Stich *et al.* [111] and in the TB-MD study of Servalli *et al.* [109]. In other theoretical papers cooling of l-Si is even performed in a N, V, T ensemble with a fixed

volume that corresponds to the experimental density of c-Si, see e.g. Refs. 107 and 113. That means that also other attempts to prepare realistic a-Si had to use an empirical input in order to get a-Si with a characteristic tetrahedral short-range order. Finally it must be noticed that in MD simulation of SPER and SD in Secs. IV and V SW-type potentials of Balamane *et al.* with values of λ greater than λ_0 ($\lambda = 1.2\lambda_0, 1.3\lambda_0, 1.4\lambda_0, 1.5\lambda_0$) are considered, without using a temperature dependence as in Eqs. (1) and (2). For more details on this topic the reader is referred to these sections.

B. Tersoff (T)-type interatomic potentials

1. T3 potential [35]

The interatomic potential denoted in Ref 35 by "C" is usually called Tersoff 3 or T3 potential (see Supplementary Material [81]). Melting of c-Si (at 3000 K) and cooling leads to a-Si with structural properties that agree well with available experimental and theoretical data, with the exception of the heat of crystallization that is higher than the experimental value (see Tables I, II, and III). The calculated melting point of a-Si and the heat of melting are 2050 K and 0.18 eV, respectively, with a density increase of 7.2%. As already discussed in several papers, these results do not agree with measurements. Presentations similar to Figs. 1 and 2 are shown in the Supplementary Material [81].

2. Modified T potential of Kumagai et al. (KMOD) [105]

These authors used a modified Tersoff potential, called "MOD" in their paper, in order to obtain improvements for melting temperature and elastic constants of c-Si. Kumagai *et al.* [105] introduced a new bond-angle dependent function into the bond-order term, changed the cutoff function, and performed a complete re-parametrization (see Supplementary Material [81]). In the present work melting of c-Si was performed at 2700 K, followed by cooling within the framework of the isobaric-isothermal ensemble, and subsequent equilibration at 300 K. Amorphous Si with realistic structural properties was obtained (see Tables I, II, and III), with the exception of atomic density and heat of crystallization that are too high. The bond angle distribution (see Supplementary Material [81]) shows an asymmetry with respect to the tetrahedral angle and a small peak at 60° which may be related to three-member rings [83]. Similar, but less pronounced features are also found in the case of the T3 potential. The melting temperature (1350 K) is not far from the experimental value whereas the heat of melting (0.091 eV) is much too low. The density increase upon melting is 12%. A compilation of all results can be found in the Supplementary Material [81]). Present results are in agreement with data of Schelling [108] who used the KMOD potential to determine structural, thermal, and kinetic properties of a-Si.

IV. MD SIMULATION OF SPER

The method of MD simulation of planar SPER (into the [100] direction) used here is similar to that described in a former paper [40]. The main topics are summarized in the following. The simulation cell is a cuboid with a long side parallel to [100] and two short sides parallel to [010] and [001]. The cell contains 3000 atoms and has the dimensions $15d \times 5d \times 5d$ .Three-dimensional periodic boundary conditions are employed. The simulation cell is subdivided along the x-axis into an inner part and an outer part. The inner part extends from $-0.5 f L_x$ to $+0.5 f L_x$, with $L_x = 15d$ and $f < 1$. The two parts are coupled to different Berendsen thermostats, and zero pressure is maintained at the cell boundaries at $-L_x$ and $+L_x$ using a Berendsen barostat [65]. At the beginning, in the whole cell the atomic arrangement corresponds to that in c-Si. In order to prepare a sample with an amorphous inner part and a single-crystalline outer part, the inner part is heated up well above the melting point, whereas the thermostat coupled to the outer part has a temperature of 300 K. Then cooling of the inner part is performed using methods similar to those described in Sec. III A for the different interatomic potentials. Finally, inner and outer parts of the simulation cell consist of a-Si and c-Si, respectively, with a temperature of 300 K in the whole material. This system can be used as model for the real situation with an amorphous surface layer and a single-crystalline substrate. The present configuration contains two a-c interfaces. This has the advantage that statistical fluctuations occurring during SPER in this small atomic system can be somewhat reduced by determining the SPER velocity as mean value of the results for the two interfaces.

In order to distinguish atoms of the crystalline part from atoms of the amorphous part the following characterization method is applied to the configuration obtained as the results of the above preparation procedure: During an additional equilibration step at 300 K time averages of the atomic coordinates are calculated over periods of $\Delta t_{\mathrm{av}} = 2$ ps. From these data the bond angles are obtained for the averaged system. The time average eliminates the thermal vibrations of atoms and reveals the inherent structure [119]. In the case of c-Si the inherent structure shows a much narrower bond angle distribution than the instantaneous structure at a given temperature. On the other hand, in a-Si the disorder is not really determined by thermal vibrations but almost exclusively due to the amorphous structure itself. Therefore, the time average does not significantly change the bond angle distribution in a-Si. Based on time averages of the atomic coordinates the following criteria are used to assign an atom to the crystalline part: (i) The atom has four nearest neighbors within the cutoff distance of 2.95 Å. (ii) The maximum deviation of the cosine of all bond angles from the ideal value $-\frac{1}{3}$ defined by the diamond structure must not exceed the threshold $\Delta \cos_{\mathrm{th}} = 0.1$. (iii) Two or more nearest neighbors of the atom belong to the crystalline part. (iv) Three or more second nearest neighbors belong to the crystalline part. Note that the values of Δt_{av} and $\Delta \cos_{\mathrm{th}}$ as well as the other criterion are the result of several attempts, including visualization, which aimed at an optimal characterization. The ability of the above characterization procedure to distinguish between atoms of the crystalline and the amorphous material is demonstrated in Fig. 4. This

figure shows results of MD simulations with the SW-type potential of Balamane *et al.* (see Sec. III A 1). Fig. 4 (a) depicts the inherent structure determined by time averaging. Well separated amorphous and crystalline layers are found**.** The simulation cell comprises about 62.5 % amorphous and 37.5% crystalline material. Structures like that depicted in Fig. 4 (a) are used as start configurations in the simulation of the recrystallization process at different temperatures. Fig. 4 (b) depicts the crystalline fraction in dependence on the x-coordinate for the system given in Fig. 4 (a). The pair correlation function and the bond angle distribution for the amorphous and crystalline part of Fig. 4 (a) are displayed in Figs. 4 (c) and (d). These characteristics are shown for the inherent structures.

In MD simulations of SPER the whole cell is coupled to one Berendsen thermostat, and zero pressure is maintained at the cell boundaries at $-L_x$ and $+L_x$ using a Berendsen barostat. At first the system is heated from 300 K to the temperature at which the regrowth is to be investigated. During the simulation the characterization method based on time-averaged atomic coordinates and the criteria (i)-(iv) (see above) is continuously applied in order to distinguish between atoms belonging to the crystalline and the amorphous part and to determine the current crystalline fraction as well as the current a-c interface. The latter is obtained in the following manner: An atom is situated at the interface if it belongs to the crystalline part and if it has at least one nearest neighbor belonging to the amorphous part. Using the data on the current a-c interface, its mean position with respect to the x-axis and its roughness given by the *rms* deviation of this position is calculated throughout the simulation of recrystallization. As already mentioned above, the simulation cell contains two interfaces so that an averaging of the results is performed. It must be mentioned that the procedure to calculate the position of the a-c interface with respect to the x-axis and its *rms* deviation does only work properly if the amorphous part is contiguous and if the positions of the left and the right interfaces are at $x \leq 0$ and $x > 0$, respectively. Both conditions are in agreement with the purpose of the SPER simulations to be performed in this work. Also, pair correlation functions and the bond angle distributions of the amorphous and the crystalline part of the simulation cell are determined for selected examples in order to monitor the SPER process. The above-mentioned procedures of analysis, including the visualization of the atomic configuration after certain SPER stages, guarantee that only the recrystallization of a-Si is considered and cases showing melting of a-Si or liquid-phase recrystallization are sorted out.

Figure 5 (a) depicts the shift of the average position of the a-c interface with respect to the *x* axis versus time for the example of recrystallization at 1050 K and in the case of simulations with the SW-type potential of Balamane *et al.* (see Sec. III A 1). In order to determine the velocity of SPER a linear fit to the curve is performed. At 1050 K the recrystallization proceeds rather continuously whereas at lower temperatures it is more discontinuous. In the latter case the role of thermal fluctuations is more obvious than at high temperatures. The development of the roughness of the a-c interface expressed by the *rms* deviation of the average position of the interface with respect to the *x* axis is shown in Fig. 5 (b). A nearly stationary value of about 0.3 nm is reached during the whole period between 0 and 24 ns. Atomic mechanisms of SPER are illustrated in Fig. 6, for the example discussed above. The a-c interface contains small {111} facets where recrystallization mainly takes place. Obviously, this process is characterized by a sequential local rearrangement of atomic bonds

and positions. This is in agreement with the well-known and above-mentioned model in which SPER proceeds on {111} terraces or facets [19-21].

Fig. 7 depicts an Arrhenius plot of the SPER velocities obtained by MD simulations using different interatomic potentials. The data were determined for three versions of the SW-type potential of Balamane *et al.* [80] (see Secs. III A 1) which differ by the value of the three-body parameter λ , and for T-type potentials of Tersoff [35] (T3, see Sec. III B 1) and Kumagai *et al.* [105] (KMOD, see Sec. III B 2). In all cases the data (shown by small symbols) can be approximately fitted to a straight line. This is in qualitative agreement with experimental findings. The thickness of the lines is larger in the temperature range in which simulations were performed. Due to limitations of computing time, simulations were only possible for SPER velocities above some 10^{-5} nm/ns. This is the reason why for some interatomic potentials the data must be calculated for temperatures where real existing a-Si is already melted but a-Si obtained by the corresponding potential is still solid. In these cases the following points must be taken into account: (i) If one assumes that the line obtained by the fit to calculated data is also valid at lower temperature, these results can be used for comparison with measurements. (ii) As described in Sec. III A 4, even in the case of SW-type potentials of Balamane *et al.* with higher values of the three-body parameter λ a realistic melting behavior can be modeled. However, such a modification of the potentials is not used here because of the above-mentioned problem regarding computing time at lower temperatures. Furthermore, Fig. 7 presents two lines obtained from the most reliable and comprehensive experimental data sets [7,11]. The line thickness is increased in the temperature range in which the measurements were carried out. Table IV shows the SPER activation enthalpy and the pre-factor obtained from simulation results and experiments. It is obvious from Table IV and Fig. 7 that SPER data calculated by many interatomic potentials do not agree with measurements. In most cases the calculated SPER velocities are too high. On the other hand, Fig. 7 demonstrates that increasing the three body parameter of SW-type potential of Balamane *et al.* from $\lambda_0 = 21$ to $1.3\lambda_0$ and $1.5\lambda_0$ decreases the SPER velocity significantly and leads to higher values of the activation enthalpy and an approach to the experimental data. However, a fully quantitative agreement could not be reached. Even in the best cases ($1.3\lambda_0$ and $1.5\lambda_0$) there are deviations, in particular at lower temperature. At this point is must be mentioned that in SPER simulations the increased values of the three-body parameter ($1.3\lambda_0$ and $1.5\lambda_0$) were only used in the amorphous part. Since the method which determines whether atoms belong to in a- or c-Si is applied throughout the simulation the forces on the atoms can be updated correspondingly. Using increased three-body parameters for both a- and c-Si was also investigated, but this did not lead to better results. On the other hand, there is no need for using a higher λ for c-Si since many properties can be described better by applying the original value. As already mentioned earlier, increasing the three-body parameter leads to a higher preference for a tetrahedral coordination of atoms. i.e. to a “higher penalty” for bond rearrangements which are required for the SPER process. The data provided by the T3 potential are about two orders of magnitude higher than those of the measurements whereas

the pre-factor is not too far from the experimental value. The results for the KMOD potential deviate strongly from the measured SPER data.

Table V gives an overview on the physical simulation time at the respective temperature. In order to obtain a kind of stationary SPER regime, a moderate size of the MD cell but long periods of SPER simulations are preferred. This leads to weeks and months of real computing time. In the case of lower temperatures a number of independent simulations were performed, with different heating rates and different arrangements of the heat bath. Despite these efforts, the statistical error of the results for low temperatures is higher than that for high temperatures. As a crude estimation, this may lead to an error of the activation enthalpy in the order of 10 %. Furthermore, one should keep in mind that the finite dimension of the simulation cell may cause the suppression or the preference of certain regrowth modes which are mainly determined by the boundary conditions perpendicular to the main recrystallization direction. In previous MD simulations of SPER of a-Ge [40] it was found that the cell size might slightly influence (increase) the absolute value of SPER velocity but does not affect significantly the activation enthalpy.

V. MD SIMULATION OF SD

The atomic mobility in a-Si is investigated within the framework of the isobaric-isothermal ensemble (N,P,T with $P=0$) by calculating the time dependence of the atomic mean squared displacement $MSD(t)$

$$MSD(t)=\frac{1}{N}\sum_{i=1}^{N}[\mathbf{r}_i(t)-\mathbf{r}_i(0)]^2 \qquad (3)$$

where $\mathbf{r}_i(0)$ is the position of atom i at the beginning of the diffusion simulation and $\mathbf{r}_i(t)$ is the position at time t. The self-diffusion coefficient D is obtained by employing the Einstein relation

$$D=\lim_{t\to\infty}\frac{MSD(t)}{6t} \qquad (4)$$

In practice, at first $MSD(t)$ is fitted to a linear function of time and then D is obtained from the slope. Due to the nature of thermal fluctuations, at high temperature $MSD(t)$ increases continuously with time, whereas a more and more discontinuous behavior is observed at lower temperatures. This is very similar to the time dependence of the SPER velocity [Fig. 5 (a)]. It should be noticed that in a-Si all atoms may contribute to the self-diffusion coefficient whereas in c-Si only atoms in the environment of vacancies and self-interstitials are relevant. In order to obtain a statistically significant value of D, MD simulations must be carried out for a suitable time that strongly depends on the interatomic potential and the temperature. In most cases a

cubic simulation cell with 1000 atoms and periodic boundary conditions were used. In selected cases calculations with a larger cube consisting of 4096 atoms were performed.

Figs. 8 (a) and (b) show the self-diffusion coefficients obtained for the different interatomic potentials. In order to obtain the data of Fig. 8 (a) four versions of the interatomic potential of Balamane *et al.* [80] (see Sec. III A 1) were used which differ by the value of the three-body parameter λ . The simulation results are depicted by small circles. In all cases the self-diffusion coefficient can be fitted to straight lines in the Arrhenius-type representation which is in qualitative agreement with experiments. The black line shows the fit to the experimental data of Ref. 6. The temperature range where experimental investigations or simulations were performed are marked by thick lines. Due to limitations of computing time, simulations were only possible for self-diffusion coefficients above about 10^{-13} cm^2/s. For some interatomic potentials results of the simulations are shown for temperatures higher than the melting point of real existing a-Si. The reason is similar to that for the corresponding SPER simulations, see the discussion in Sec. IV. The values of the SD activation enthalpy and the pre-exponential factor are summarized in Table VI. This table and Figs. 8 (a) and (b) indicate that the SD coefficients calculated by simulations with different interatomic potentials are often much higher than the experimental data. Like in SPER simulations, D can be reduced and the activation enthalpy can be increased by using SW-type potentials of Balamane *et al.* with higher values of the three body parameter. But a fully quantitative agreement cannot be obtained. Although the data determined using SW-type potentials Balamane *et al.* with $\lambda = 1.3\lambda_0$, $1.4\lambda_0$ and $1.5\lambda_0$ are close to the experimental line at high temperature, deviations occur in the temperature range where the SD experiments were performed. As in the case of SPER, increasing λ leads to a reduction of local bond rearrangements which are also required for the SD process. The use of the SW-type potentials of Vink *et al.* [103] (see Sec. III A 2) and Albenze *et al.* [104] (see Sec. III A 3) does not yield satisfactory results. On the other hand, the activation enthalpy determined for the T3 potential [35] (see Sec. III B 1) is closest to the experimental value but the SD coefficient is more than two orders of magnitude too high. The KMOD potential of Kumagai [105] (see Sec. III B 2) yields self-diffusion data which are much higher than the measured ones.

The atomic mechanisms of SD in a-Si were intensively studied and simple and complex bond rearrangements, such as bond defect formation and dissolution as well as modified concerted exchanges were found. Results of these detailed studies will be the subject of another paper.

The physical simulation times for the respective calculations are summarized in Table VII. As in the case of SPER a moderate size of the simulation cell was chosen, but long MD simulations were performed in order to determine the SD coefficient for a sufficiently stationary diffusion regime. Therefore the real computing time was very high and comprised weeks and months. Nevertheless, one should notice that the statistical error of D is higher at low temperatures. Therefore, similarly to SPER simulation, the estimated uncertainty of the value for the activation enthalpy is in the order of 10 %. For the SW potential of Balamane *et al.* [80] SD simulations were also performed for the larger supercell containing 4096 atoms. The calculated value of D is slightly higher than that for a system with 1000 atoms. However, the activation enthalpy is not very different (see Supplementary Material [81]).

Furthermore, it was investigated whether a preexisting vacancy (V) or self-interstitial (I) may influence self-diffusion in a-Si. For this purpose an atom was removed or added to the supercell with 1000 atoms and a subsequent energy minimization was performed under zero pressure conditions. In the case of the SW potential of Balamane *et al.* [80] V formation enthalpy and the formation volume are 0.54 eV and -13.9 Å^3, respectively, whereas 3.04 eV and +16.4 Å^3 were obtained for I. Subsequently, SD simulations were carried out at 800 and 1000 K using the isobaric-isothermal ensemble (N,P,T with $P=0$). The results depicted by large symbols in Fig. 8 (a) are very close to the data points calculated for a simulation cell without any V or I. Such a close agreement is also found for the corresponding SW-type potential with $\lambda = 1.4\lambda_0$ and for temperatures of 1500 and 2000 K. These findings demonstrate that in the relatively open amorphous Si structure SD does not change significantly if one atom is removed or added. Obviously, these perturbations are "neutralized" or "eaten" relatively fast by the amorphous material. This is in contrast to the single crystal where the solid is rather rigid so that V or I exist permanently, and realistic SD is only possible by these defects.

VI. CONCLUSIONS

The comprehensive overview on the state of the art in the research on SPER and SD in a-Si led to the question whether both phenomena are determined by very similar processes as this was already discussed qualitatively by some authors. In the present work MD simulations with several SW- and T-type interatomic potentials were performed to check this issue. Before use of the potentials in SPER and SD calculations, the procedure for preparation of a-Si was outlined and its properties were studied. A good or satisfactory agreement with structural data measured at room temperature was found, but the thermal properties show larger deviations from experimental results.

The comparison between results of MD simulations of SPER and SD clearly shows the similarity of the activation enthalpies obtained for the respective interatomic potentials, see Tables IV and VI. That means that the present MD simulations obviously demonstrate that SPER and SD are governed by the same or very similar atomic processes. While the activation enthalpies for SPER and SD obtained for a respective SW-type potential agree well, the use of T-type potentials leads to slight deviations. Present results also indicate that the atomic jumps occurring during SD in a-Si are responsible for SPER, mainly those close to the a/c interface. On the other hand, in SPER simulations c-Si can be assumed to be completely rigid, with the exception of thermal vibration of the atoms which does not contribute to atomic migration. Furthermore, present findings are consistent with experiments on SPER of a-Ge in which local bond rearrangements near the interface were found to be responsible for the recrystallization [15]. It must be noticed that SPER competes with SD so that in the investigations reported in Ref. 15 SPER was too fast so that significant SD in a-Ge could not be observed. The results of present work indicate that the interatomic potentials used are able to describe both processes qualitatively but not quantitatively. An improved agreement with

measured data for SPER and SD can be obtained for SW-type potentials of Balamane *et al.* [80] (see Sec. III A 1) if for a-Si an increased value for the three-body parameter is used. In these cases MD simulations require tremendous computing times of weeks and months which correspond to physical times up to some microseconds. To the best of our knowledge such kind of long MD simulations have not hitherto carried out in the case of a-Si. The necessity to employ MD simulations is due to the fact that in a-Si a lot of different individual barriers exist. This is in contrast to single-crystalline materials where the lattice structure limits the number of barriers so that diffusion coefficients can be often calculated by more effective methods than MD simulations. Results of detailed studies on atomic mechanisms of SD in a-Si will be presented in another paper.

Present work also demonstrates the well-known limited transferability of classical interatomic potentials: The potentials are fitted to a certain number of data obtained by experiments or first-principle calculations which does not guarantee that MD simulations of phenomena outside the range of the fit lead to reasonable quantitative results. However, using the interatomic potentials investigated here, SPER and SD can be described at least qualitatively, and in some cases the results are even not too far from experimental data. In future work, recently developed interatomic potentials which are based on machine-learning methods (i.e. on a flexible collection of data, see e.g. Ref. 101) should be checked if they are able to calculate by higher precision SPER and SD as well as “conventional” structural and thermal properties of a-Si.

SUPPLEMENTARY MATERIAL

See supplementary material [81] for (i) details on the interatomic potentials considered and the structural and thermal properties of a-Si calculated using these potentials, and (ii) the influence of the size of the simulation cell on the MD results for SD in a-Si.

ACKNOWLEDGMENTS

M. Posselt is grateful for funding by the Deutsche Forschungsgemeinschaft (DFG) via PO436/9-1, H. Bracht and D. Radić for funding by DFG via BR 1520/21-1.

CONFLICT OF INTEREST

The authors have no conflicts to disclose.

DATA AVAILABILITY

The data that support the findings of this study are available from the corresponding author upon reasonable request.

REFERENCES

[1] B. J. Pawlak, R. Surdeanu, B. Colombeau, A. J. Smith, N. E. B. Cowern, R. Lindsay, W. Vandervorst, B. Brijs, O. Richard, and F. Cristiano, Evidence on the mechanism of boron deactivation in Ge-preamorphized ultrashallow junctions, Appl. Phys. Lett. **84**, 2055 (2004).

[2] B. J. Pawlak, T. Janssens, B. Brijs, W. Vandervorst, E. J. H. Collart, S. B. Felch, and N. E. B. Cowern, Effect of amorphization and carbon co-doping on activation and diffusion of boron in silicon, Appl. Phys. Lett. **89**, 062110 (2006).

[3] M. J. Powell, The physics of amorphous-silicon thin-film transistors, IEEE Trans. Electron. Devices **36,** 2753 (1989).

[4] A. Shah, Photovoltaic technology: The case for thin-film solar cells, Science **285,** 692 (1999).

[5] M. T. McDowell, S. W. Lee, W. D. Nix, and Y. Cui, Understanding the lithiation of silicon and other alloying anodes for lithium-ion batteries, Adv. Mater. **25,** 4966 (2013).

[6] J. Kirschbaum T. Teuber, A. Donner, M. Radek, D. Bougeard, R. Böttger, J. Lundsgaard Hansen, A. Nylandsted Larsen, M. Posselt, and H. Bracht, Self-diffusion in amorphous silicon by local bond rearrangements, Phys. Rev. Lett. **120,** 225902 (2018).

[7] G. L. Olson and J. A. Roth, Kinetics of solid phase crystallization in amorphous silicon, Mater. Sci. Rep. **3**, 1 (1988)

[8] B. C. Johnson, J. C. McCallum, and M. J. Aziz, in *Handbook of Crystal Growth, Thin Films and Epitaxy: Basic Techniques, vol. III, Part A, Second Edition* (Elsevier Amsterdam, Boston, Heidelberg, London, New York, Oxford, Paris, San Diego, San Francisco, Singapore, Sydney, Tokyo, 2015) pp.317-363.

[9] L. Csepregi, E. F. Kennedy, J. W. Mayer, and T. W. Sigmon, Substrate-orientation dependence of the epitaxial regrowth from Si-implanted amorphous Si, J. Appl. Phys. **49**, 3906 (1978).

[10] A. Lietoila, A. Wakita, T. W. Sigmon, and J. F. Gibbons, Epitaxial regrowth of intrinsic, ^{31}P-doped and compensated (^{31}P+^{11}B-doped) amorphous Si, J. Appl. Phys. **53**, 4339 (1982).

[11] J. A. Roth, G. L. Olson, D. C. Jacobson, J. M. Poate, Kinetics of solid phase epitaxy in thick amorphous Si layers formed by MeV ion implantation, Appl. Phys. Lett. **57**, 1340 (1990).

[12] G.-Q. Lu, E. Nygren, and M. J. Aziz, Pressure-enhanced crystallization kinetics of amorphous Si and Ge: Implications for point-defect mechanisms, J. Appl. Phys. **70**, 5323 (1991).

[13] S. Roorda, and Y. Lavigueur, Solid phase epitaxial regrowth of amorphous silicon is not affected by structural relaxation, Philos. Mag. **90**, 3787 (2010).

[14] J.A. Roth, G. L. Olson, D. C. Jacobson, J. M. Poate, and C. Kirschbaum, The effect of hydrogen on the kinetics of solid phase epitaxy in amorphous silicon, Mater. Res. Soc. Symp. Proc. **205**, 45 (1992).

[15] M. Radek, H. Bracht, B. C. Johnson, J. C. McCallum, M. Posselt, and B. Liedke, Atomic transport during solid-phase epitaxial recrystallization of amorphous germanium, Appl. Phys. Lett. **107**, 082112 (2015).

[16] F. Spaepen, A structural model for the interface between amorphous and crystalline Si or Ge, Acta Mater. **26**, 1167 (1978).

[17] T. Saito and I. Ohdomari, A structural model for the interface between amorphous and (100) crystalline silicon, Philos. Mag. B **43**, 673 (1981).

[18] R. Drosd and J. Washburn, Some observations on the amorphous to crystalline transformation in silicon, J. Appl. Phys, **53**, 397 (1982).

[19] J. S. Williams and R. G. Elliman, Role of electronic processes in epitaxial recrystallization of amorphous semiconductors, Phys. Rev. Lett. **51**, 1069 (1983).

[20] E. Rimini, *Ion implantation: Basics to Device Fabrication* (Kluwer Academic Publishers, Boston, Dordrecht, London 1994).

[21] J. M. Poate and J. S. Williams, in *Ion Implantation and Beam Processing* (Academic Press, New York, 1984), pp. 13–57.

[22] N. Bernstein, M. A. Aziz, and E. Kaxiras, Amorphous-crystal interface in silicon: A tight-binding simulation, Phys. Rev. B **58**, 4579 (1998).

[23] L. A. Marques, L. Pelaz, M. Aboy, L. Enriquez, and J. Barbolla, Microscopic description of

the irradiation-induced amorphization in silicon, Phys. Rev. Lett. **91**, 135504 (2003).

[24] L. Pelaz. L. A. Marques, and J. Barbolla, Ion-beam-induced amorphization and recrystallization in silicon, J. Appl. Phys. **96**, 5947 (2004).

[25] I. Martin-Bragado, and V. Moroz, Facet formation during solid phase epitaxy regrowth: A lattice kinetic Monte Carlo model, Appl. Phys. Lett. **95**, 123123 (2009).

[26] I. Martin-Bragado and B. Sklenard, Understanding Si (111) solid phase epitaxial regrowth using Monte Carlo modeling: Bi-modal growth, defect formation, and interface topology, J. Appl. Phys. **112**, 024327 (2012).

[27] I. Martin-Bragado, Importance of twin defect formation created by solid-phase epitaxial growth: An atomistic study, Scr. Mater. **66**, 186 (2012).

[28] N. Bernstein, M. J. Aziz, and E. Kaxiras, Atomistic simulations of solid-phase epitaxial growth in silicon, Phys. Rev. B **61**, 6696 (2000).

[29] T. Motooka, K. Nisihira, S. Munetoh, K. Moriguchi, and A. Shintani, Molecular-dynamics simulations of solid-phase epitaxy of Si: Growth mechanisms, Phys. Rev. B **61**, 8537 (2000).

[30] K. Gärtner and B. Weber, Molecular dynamics simulations of solid-phase epitaxial growth in silicon, Nucl. Instrum. Methods B **202**, 255 (2003).

[31] A. Mattoni and L. Colombo, Boron ripening during solid-phase epitaxy of amorphous silicon, Phys. Rev. B **69**, 045204 (2004).

[32] C. Krzeminski, Q. Brulin, V. Cuny, E. Lecat, E. Lampin, and F. Cleri, Molecular dynamics simulation of the recrystallization of amorphous Si layers: Comprehensive study of the dependence of the recrystallization velocity on the interatomic potential, J. Appl. Phys. **101**, 123506 (2007).

[33] E. Lampin and C. Krzeminski, Molecular dynamics simulations of the solid phase epitaxy of Si: Growth mechanism and orientation effects, J. Appl. Phys. **106**, 063519 (2009).

[34] C. Krzeminski and E. Lampin, Solid phase epitaxy amorphous silicon re-growth: some insight from empirical molecular dynamics simulation, Eur. Phys. J. B **81**, 283 (2011).

[35] J. Tersoff, Empirical interatomic potential for silicon with improved elastic properties, Phys. Rev. B **38**, 9902 (1988).

[36] K. V. Shanavas, K. K. Pandey, N. Garg, and S. M. Sharma, Computer simulations of crystallization kinetics in amorphous silicon under pressure, J. Appl. Phys. **111**, 063509 (2012).

[37] T. Saito and I. Ohdomari, Quantitative analysis of the bond rearrangement process during solid phase epitaxy of amorphous silicon, Philos. Mag. B **49**, 471 (1984).

[38] B. Weber, D. M. Stock, and K. Gärtner, MD simulations of ion beam induced epitaxial crystallization at a-Si/c-Si interfaces: Interface structure and elementary processes of crystallization, Nucl. Instrum. Methods. B **148**, 375 (1999).

[39] D. M. Stock, B. Weber, and K. Gärtner, Role of the bond defect for structural transformations between crystalline and amorphous silicon: A molecular-dynamics study, Phys. Rev. B **61**, 8159 (2000).

[40] M. Posselt and A. Gabriel, Atomistic simulation of amorphous germanium and its solid phase epitaxial recrystallization, Phys. Rev. B **80**, 045202 (2009).

[41] F. Strauß, L. Dörrer, T. Geue. J. Stahn, A. Koutsioubas, S. Mattauch, and H. Schmidt, Self-diffusion in amorphous silicon, Phys. Rev. Lett. **116,** 025901 (2016), Erratum: Phys. Rev. Lett. **116,** 089903 (2016).

[42] S. Roorda, J. S. Custer, W. C. Sinke, J. M. Poate, D. C. Jacobson, A. Polman, and F. Spaepen, Structural relaxation in amorphous silicon and the role of network defects, Nucl. Instrum. Methods B **59–60**, 344 (1991).

[43] M. A. Noah, D. Flötotto, Z. Wang, and E. J. Mittemeijer, Concentration-dependent self-diffusion coefficients in a-$Si_{1-x}Ge_x$ solid solutions: An interdiffusion study, J. Appl. Phys. **117**, 165306 (2015).

[44] S. M. Prokes and F. Spaepen, Interdiffusion in Si/Ge amorphous multilayer films, Appl. Phys. Lett. **47**, 234 (1985).

[45] P. D. Persans and A. F. Ruppert, Atomic interdiffusion in amorphous silicon and germanium, Mater. Res. Soc. Symp. Proc. **57**, 329 (1987).

[46] C. Janot, A. Bruson, and G. Marchal, Neutron scattering measurements of interdiffusion in amorphous Si/Ge multilayers, J. Phys. (Paris) **47**, 1751 (1986).

[47] J. Gonzalez-Hernandez, D. D. Allred, and O. V. Nguyen, Anneal induced changes in

amorphous semiconductor multilayers, Mater. Res. Soc. Symp. Proc. **77**, 665 (1987).

[48] S. D. Theiss, F. Spaepen, and M. J. Aziz, Pressure-enhanced interdiffusion in amorphous Si/Ge multilayers, Appl. Phys. Lett. **68**, 1226 (1996).

[49] A. Simon, A. Csik, F. Paszti, A. Z. Kiss, D. L. Beke, L. Daroczi, Z. Erdelyi, and G. A. Langer, Study of interdiffusion in amorphous Si/Ge multilayers by Rutherford backscattering spectrometry, Nucl. Instrum. Methods B **161-163**, 471 (2000).

[50] A. Csik, G. A. Langer, D. L. Beke, Z. Erdelyi, M. Menyhard, and A. Sulyok, Interdiffusion in amorphous Si/Ge multilayers by Auger depth profiling technique, J. Appl. Phys. **89**, 804 (2001).

[51] A. Csik, D. L. Beke, G. A. Langer, Z. Erdelyi, L. Daroczi, K. Kapta, and M. Kis-Varga, Non-linearity of diffusion in amorphous Si-Ge multilayers, Vacuum **61**, 297 (2001).

[52] J. A. Roth, G. L. Olson, D. C. Jacobson, and J. M. Poate, Diffusion of hydrogen in amorphous silicon in the low concentration regime, Mater. Res. Soc. Symp. Proc. **297**, 291 (1993).

[53] V. C. Venezia, R. Duffy, L. Pelaz, M. J. P. Hopstaken, G. C. J. Maas, T. Dao, Y. Tamminga, and P. Graat, Boron diffusion in amorphous silicon, Mat. Sci. Eng. B **124-125**, 245 (2005).

[54] S. Mirabella, D. De Salvador, E. Bruno, E. Napolitani, E. F. Pecora, S. Boninelli, and F. Priolo, Mechanism of boron diffusion in amorphous silicon, Phys. Rev. Lett. **100**, 155901 (2008).

[55] S. T. Pantelides, Defects in amorphous Silicon: A new perspective, Phys. Rev. Lett. **57**, 2979 (1986).

[56] Y. Song, R. Malek, and N. Mousseau, Optimal activation and diffusion paths of perfect events in amorphous silicon, Phys. Rev. B **62**, 15680 (2000).

[57] F. H. Stillinger and T. A. Weber, Computer simulation of local order in condensed phases of silicon, Phys. Rev. B **31**, 5252 (1985).

[58] G. T. Barkema and N. Mousseau, Identification of relaxation and diffusion mechanisms in amorphous silicon, Phys. Rev. Lett. **81**, 1865 (1998).

[59] N. Mousseau and G. T. Barkema, Traveling through potential energy landscapes of disordered materials: The activation-relaxation technique, Phys. Rev. E **57**, 2419 (1998).

[60] F. Wooten, K. Winer, and D. Weaire, Computer generation of structural models of amorphous Si and Ge, Phys. Rev. Lett. **54**, 1392 (1985).

[61] S. Sastry, and C. A. Angell, Liquid–liquid phase transition in supercooled silicon, Nat. Mater. **2**, 739 (2003).

[62] I. Santos, L. A. Marques, L. Pelaz, and L. Colombo, Elucidating the atomistic mechanisms driving self-diffusion of amorphous Si during annealing, Phys. Rev. B **83**, 153201 (2011) .

[63] Y. Limoge and J. L. Bocquet, Temperature behavior of tracer diffusion in amorphous materials: A random-walk approach. Phys. Rev. Lett. **65**, 60 (1990).

[64] K. Mussawisade, T. Wichmann, and K.W. Kehr, Combination of random-barrier and random-trap models. J. Phys. Condens. Matter **9**, 1181 (1997).

[65] H. J. C. Berendsen, J. P. M. Postma, W. F. van Gunsteren, A. DiNola, and J. R. Haak, J. Chem. Phys. **81**, 3684 (1984).

[66] J. F. Justo, M. Z. Bazant, E. Kaxiras, V. V. Bulatov, S. Yip, Interatomic potential for silicon defects and disordered phases, Phys. Rev. B **58**, 2539 (1998).

[67] M. I. Baskes, J. S. Nelson, and A. F. Wright, Semiempirical modified embedded-atom potentials for silicon and germanium, Phys. Rev. B **40,** 6085 (1989).

[68] T. J. Lenosky, B. Sadigh, E. Alonso, V. V. Bulatov, T. Diaz de la Rubia, J. Kim, A. F. Voter, and J. D. Kress, Highly optimized empirical potential model of silicon, Model. Simul. Mater. Sci. Eng. **8**, 825 (2000).

[69] Y. A. Du, T. J. Lenosky, R. G. Hennig, S. Goedecker, and J. W. Wilkins, Energy landscape of silicon tetra-interstitials using an optimized classical potential, Phys. Status Solidi B **248**, 2050 (2011).

[70] B.-J. Lee, A modified embedded atom method interatomic potential for silicon, CALPHAD: Comput. Coupling of Ph. Diagr. Thermochem. **31**, 95 (2007).

[71] S. Ryu, C. R. Weinberger, M. I. Baskes, and W. Cai, Improved modified embedded-atom method potentials for gold and silicon, Model. Simul. Mater. Sci. Eng. **17**, 075008 (2009).

[72] X. Huang, X. Dong, L. Liu, and P. Li, An improved modified embedded-atom method potential to fit the properties of silicon at high temperature, Comput. Mater. Sci. **153**, 251 (2018).

[73] P. Erhart and K. Albe, Analytical potential for atomistic simulations of silicon, carbon, and silicon carbide, Phys. Rev. B **71**, 035211 (2005).

[74] B. A. Gillespie, X. W. Zhou, D. A. Murdick, H. N. G. Wadley, R. Drautz, and D. G. Pettifor, Bond-order potential for silicon, Phys. Rev. B **75**, 155207 (2007).

[75] J. D. Schall, G. Gao, and J. A. Harrison, Elastic constants of silicon materials calculated as a function of temperature using a parametrization of the second-generation reactive empirical bond-order potential, Phys. Rev. B **77**,115209 (2008).

[76] G. P. P. Pun and Y. Mishin, Optimized interatomic potential for silicon and its application to thermal stability of silicene, Phys. Rev. B **95**, 224103 (2017).

[77] A. P. Bartók, J. Kermode, N. Bernstein, and G. Csányi, Machine learning a general-purpose interatomic potential for silicon, Phys. Rev. X **8**, 041048 (2018).

[78] E. Sanville, A. Bholoa, R. Smith, and S. D. Kenny, Silicon potentials investigated using density functional theory fitted neural networks, J. Phys.: Condens. Matter **20**, 285219 (2008).

[79] E. B. Tadmor, R. S. Elliott, J. P. Sethna, R. E. Miller, and C. A. Becker, Knowledgebase of interatomic models (KIM), https://openkim.org/

[80] H. Balamane, T. Halicioglu, and W. A. Tiller, Comparative study of silicon empirical interatomic potentials, Phys. Rev. B **46**, 2250 (1992).

[81] Supplementary Material at [URL will be inserted by publisher]

[82] W. D. Luedtke and U. Landman, Preparation and melting of amorphous silicon by molecular-dynamics simulations, Phys. Rev. B **37**, 4656 (1988).

[83] E. Holmström, B. Haberl, O. H. Pakarinen, K. Nordlund, F Djurabekova, R. Arenal, J. S. Williams, J. E. Bradby, T. C. Petersen, and A. C. Y. Liu, Dependence of short and intermediate-range order on preparation in experimental and modeled pure a-Si, J. Non-Cryst. Solids **438**, 26 (2016).

[84] E. P. Donovan, F. Spaepen, J. M. Poate, and D. C. Jacobson, Homogeneous and

interfacial heat releases in amorphous silicon, Appl. Phys. Lett. **55**, 1516 (1989).

[85] E. P. Donovan, F. Spaepen, D.Turnbull, J. M. Poate, and D. C. Jacobson, Calorimetric studies of crystallization and relaxation of amorphous SI and Ge prepared by ion implantation, J. Appl. Phys. **57**, 1795 (1985).

[86] S. Roorda, S. Doorn, W. C. Sinke, P. M. L. O. Scholte, and E. van Loenen, Calorimetric evidence for structural relaxation in amorphous silicon, Phys. Rev. Lett. **62**, 1180 (1989).

[87] S. Roorda, W. C. Sinke, J. M. Poate, D. C. Jacobson, S. Dierker, B. S. Dennis, D. J. Eaglesham, F. Spaepen, and P. Fuoss, Structural relaxation and defect annihilation in pure amorphous silicon, Phys. Rev. B **44**, 3702 (1991).

[88] J. S. Custer, M. O. Thompson, D. C. Jacobson, J. M. Poate, S. Roorda, W.C. Sinke, and F. Spaepen, Density of amorphous Si, Appl. Phys. Lett. **64**, 437 (1994).

[89] K. Laaziri, S. Roorda, and J. M. Baribeau, Density of amorphous Si_xGe_{1-x} alloys prepared by high-energy ion implantation, J. Non-Cryst. Solids **191**, 193 (1995).

[90] K. Laaziri, S. Kycia, S. Roorda, M. Chicoine, J. L. Robertson, J. Wang, and S. C. Moss, High resolution radial distribution function of pure amorphous silicon, Phys. Rev. Lett. **82**, 3460 (1999).

[91] K. Laaziri, S. Kycia, S. Roorda, M. Chicoine, J. L. Robertson, J. Wang, and S. C. Moss, High-energy x-ray diffraction study of pure amorphous silicon, Phys. Rev. B **60**, 13520 (1999).

[92] J. Fortner and J. S. Lannin, Radial distribution functions of amorphous silicon, Phys. Rev. B **39**, 5527(R) (1989).

[93] S. Kugler, G. Molnar, G. Petö, E Zsoldos, L. Rosta, A. Menelle, and R. Bellissent, Neutron-diffraction study of the structure of evaporated pure amorphous silicon, Phys. Rev. B **40**, 8030 (1989).

[94] F. Kail, J. Farjas, P. Roura, C. Secouard, O. Nos, J. Bertomeu, and P. Roca i Cabarrocas, The configurational energy gap between amorphous and crystalline silicon, Phys. Stat. Sol. Rapid Res. Lett. **5**, 361 (2011).

[95] B. Haberl, A. C. Y. Liu, J. E. Bradby, S. Ruffell, J. S. Williams, and P. Munroe, Structural characterization of pressure-induced amorphous silicon, Phys. Rev. B **79**, 155209 (2009).

[96] P. F. McMillan, Relaxing times for silicon, Nat. Mater. **3**, 755 (2004).

[97] A. Hedler, S. L. Klaumünzer, and W. Wesch, Amorphous silicon exhibits a glass transition, Nat. Mater. **3**, 804 (2004).

[98] P. F. McMillan, M. Wilson, D. Daisenberger, and D. Machon, A density-driven phase transition between semiconducting and metallic polyamorphs of silicon, Nat. Mater. **4**, 680 (2005).

[99] T. Morishita, Isothermal-isobaric first-principle molecular dynamics: Application to polymorphism in liquid and amorphous materials, Mol. Simul. **33**, 5 (2007).

[100] R. Xie, G. G. Long, S. J. Weigand, S. C. Moss, T. Carvalho, S. Roorda, M. Heijna, S. Torquato, and P. J. Steinhardt, Hyperuniformity in amorphous silicon based on the measurement of the infinite-wavelength limit of the structure factor, Proc. Natl. Acad. Sci. USA **110**, 13250 (2013).

[101] V. L. Deringer, N. Bernstein, A. P. Bartok, M. J. Cliffe, R. N. Kerber, L. E. Marbella, C. P. Grey, S. R. Elliot, and G. Csanyi, Realistic atomistic structure of amorphous silicon from machine-learning-driven molecular dynamics, J. Phys. Chem. Lett. **9**, 2879 (2018).

[102] M. M. J. Treacy, J. M. Gibson, L. Fan, D. J. Paterson, and I. McNulty, Fluctuation microscopy: a probe of medium range order, Rep. Prog. Phys. **68**, 2899 (2005).

[103] R. L. C. Vink, G. T. Barkema, W. F. van der Weg, and N. Mousseau, Fitting the Stillinger-Weber potential to amorphous silicon, J. Non-Cryst. Solids **282**, 248 (2001).

[104] E. J. Albenze and P. Clancy, Interface response functions for amorphous and crystalline Si and the implications for explosive crystallization, Mol. Simul. **31**, 11 (2005).

[105] T. Kumagai , S. Izumi, S. Hara, and S. Sakai, Development of bond-order potentials that can reproduce the elastic constants and melting point of silicon for classical molecular dynamics simulation, Comput. Mater. Sci. **39**, 457 (2007).

[106] J. Tersoff, Modeling solid-state chemistry: Interatomic potentials for multicomponent systems, Phys. Rev. B **39**, 5566 (1989).

[107] M. Ishimaru, Atomistic simulations of structural relaxation processes in amorphous silicon, J. Appl. Phys. **91**, 686 (2002).

[108] P. K. Schelling, Phase behavior and kinetics of a new bond-order potential for silicon, Comput. Mater. Sci. **44**, 274 (2008).

[109] G. Servalli and L. Colombo. Simulation of the amorphous-silicon properties and their dependence on sample preparation, Europhys. Lett. **22**, 107 (1993).

[110] E. Kim and Y. H. Lee, Structural, electronic, and vibrational properties of liquid and amorphous silicon: Tight-binding molecular-dynamics approach, Phys. Rev. B **49**, 1743 (1994).

[111] I. Štich, R. Car, and M. Parrinello, Amorphous silicon studied by ab initio molecular dynamics: Preparation, structure and properties, Phys. Rev. B **44**, 11092 (1991).

[112] N. C. Cooper, C. M. Goringe, and D. R. McKenzie, Density functional theory modelling of amorphous silicon, Comput. Mater. Sci **17**, 1 (2000).

[113] H. M. Shodja, M. Tabatabaei, and K. Esfarjani, First principles molecular dynamics studies of elastic constants, ideal tensile strength, chemistry of crack initiation, and surface and cohesive energies in amorphous silicon, Philos. Mag. **94**, 2913 (2014)

[114] S. Izumi, S. Hara, T. Kumagai, and S. Sakai, Classification of amorphous-silicon microstructures by structural parameters: Molecular dynamics study, Comput. Mat. Sci. **31**, 258 (2004).

[115] A. Pedersen, L. Pizzagalli, and H. Jónsson, Optimal atomic structure of amorphous silicon obtained from density functional theory calculations, New J. Phys. **19**, 063018 (2017).

[116] R. Atta-Fynn and P. Biswas, Nearly defect-free dynamical models of disordered solids: The case of amorphous silicon, J. Chem. Phys. **148**, 204503 (2018).

[117] M. O. Thompson, G. J. Galvin, J. W. Mayer, P. S. Peercy, J. M. Poate, D. C. Jacobson, A. G. Cullis, and N. G. Chew, Melting temperature and explosive crystallization of amorphous silicon during pulsed laser irradiation, Phys. Rev. Lett. **52,** 2360 (1984).

[118] E. P. Donovan, F. Spaepen, D.Turnbull, J. M. Poate, and D. C. Jacobson, Heat of crystallization and melting point of amorphous silicon, Appl. Phys. Lett. **42**, 698 (1983).

[119] L. A. Marques, M.-J. Caturla, T. Diaz de la Rubia, and G. H. Gilmer, Ion beam induced recrystallization of amorphous silicon: A molecular dynamics study, J. Appl. Phys. **80**, 6160 (1996).

Table I. Structural properties of amorphous Si at 300 K, results of present atomistic simulations using different interatomic potentials: Atomic density n_a, relative density change with respect to c-Si $(n_a - n_c)/n_c$, mean value of the coordination number C, mean value of the bond angle θ and its *rms* deviation $\Delta\theta$, heat of crystallization of a-Si per atom ΔH_{ac}, height of the first peak of the structure factor h, difference between maximum and minimum in the distribution of the dihedral angle $\Delta g(\varphi)$.

Interatomic potentials	n_a (Å^{-3})	$\frac{n_a - n_c}{n_c}$ (%)	C	θ(°)	$\Delta\theta$(°)	ΔH_{ac} (eV)	h	$\Delta g(\varphi)$
SW, Balamane *et al.* [80]	0.04872	-2.09	4.027	108.990	10.666	0.1807	1.79	0.0057
SW, Vink *et al.* [103]	0.0476	-3.95	4.00	109.22	9.31	1.52	1.80	0.0059
SW, Albenze *et al.* [104]	0.0485	-2.29	4.032	109.00	10.78	0.138	1.79	0.0050
SW, $\lambda(T)$, Eq. (1)	0.04813	-3.22	4.039	108.97	11.11	0.260	1.69	0.0046
SW, $\lambda(T)$, Eq. (2)	0.04819	-3.11	4.039	108.95	11.32	0.269	1.73	0.0046
T, T3 [35]	0.04856	--2.12	4.048	108.96	11.82	0.189	1.59	0.0042
T, Kumagai *et al.* [105]	0.04927	-0.818	4.08	108.62	12.70	0.186	1.75	0.0040

Table II. Selected experimental data on the structure of a-Si. The quantities in the columns are explained in the caption of Table. I.

Experimental methods	n (Å^{-3})	$\frac{n_a - n_c}{n_c}$ (%)	C	θ(°)	$\Delta\theta$(°)	ΔH_{ac} (eV)	h
a-Si by self-ion implantation analysis: surface profilometry and Rutherford backscattering spectrometry in channeling direction (RBS/C)	0.0490 [88] 0.0491 [89]	-1.8 [88] -1.6 [89]					
a-Si by self-ion implantation analysis: differential scanning calorimetry / RBS/C of SPER						0.1419 [87] 0.1388 [84]	
a-Si by self-ion implantation [91] analysis: X-ray diffraction ai: as-implanted sample an: annealed sample	0.0489		3.78 (ai) 3.88 (an)	107.8 (ai) 107.8 (an)	10.45 (ai) 9.63 (an)		1.76 (an)
a-Si by self-ion implantation [100] analysis: X-ray diffraction							1.77 (an)
a-Si by rf sputtering at 100 °C [92] analysis: n-diffraction ad: as-deposited			3.4-3.5 (ad) 3.7-3.9 (an)	108.4 (ad) 108.6 (an)	11.0 (ad) 9.9 (an)		1.57 (an)
a-Si by e-beam evaporation and annealing [93]							1.87

analysis: n-diffraction							
a-Si by self-ion implantation [83] analysis: Raman spectroscopy TEM (EELS/e-diffraction)	 0.04903 (ai) 0.04909 (an)	 -1.8 -1.6	 3.7 3.9	 111.0 110.0	 10.8 (ai) 9.1 (an) 10.2 9.6	 	
a-Si by indentation (pressure) [83] analysis: Raman spectroscopy TEM/EELS (EELS/e-diffraction)	 0.04991 (ai) 0.04875 (an)	 0.0 (ai) -2.3 (an	 3.6 (ai) 3.9 (an)	 109.0 110.0	 11.5 (ai) 9.5 (an) 11.0 8.4	 	

Table III. Selected theoretical data on structural properties of a-Si from literature. Only results obtained from fast cooling of liquid Si (l-Si) are shown. For the quantities in the columns the reader is referred to Table I.

Theoretical methods	n (Å^{-3})	$\frac{n_a - n_c}{n_c}$ (%)	C	θ(°)	$\Delta\theta$(°)	ΔH_{ac} (eV)	h	$\Delta g(\varphi)$
MD using interatomic potentials								
SW potential, fast cooling of l-Si (different steps) to room temperature (RT), with temperature-dependent λ parameter, see text, 300 K N,P,T with $P=0$ [82]	0.04871		4.12	108.3	14.7			
T-type potential for SiC [106], fast cooling of l-Si to 300 K (5 K/ps), then annealing at 1400 K and cooling (5 K/ps) to 300 K N,V,T the room-temperature (RT) density of c-Si is used to determine V [107]				108.9	12.5		1.55	
KMOD potential, repeated melting and fast cooling (rate 0.91 K/ps, also lower cooling rates are considered: 0.3 K/ps and 0.15								

K/ps) N,P,T with $P=0$, structural properties for 300 K [108]	0.049543		4.12			0.193		
EDIP potential [66], fast cooling of l-Si at a rate of 10 K/ps to 77 K N,P,T with $P=0$ [83]		-2.7	4.1	107.9	17.6	0.26		0.0014
T3 potential, fast cooling of l-Si at a rate of 10 K/ps to 77 K N,P,T with $P=0$ [83]		-2.5	4.1	108.7	14.6	0.29		0.0026
GAP potential, fast cooling of l-Si (slowest rate:0.1 K/ps) to 500 K N,P,T with $P=0$ and subsequent relaxation to ground state [101]			4.00	about 109.5	11	0.14	1.75	
Tight-binding (TB) MD								
Fast cooling of l-Si (different steps) to 300 K, result for slowest cooling N,V,T with linear $V(T)$ to reproduce experimental densities of l-Si (near melting point) and of a-Si (300 K) [109]			3.99					
Fast cooling of l-Si (different steps) to 0 K			4.28	106.7	16.3	0.22		

N,V,T with V from the density of l-Si near melting point [110]								
Density-Functional-Theory (DFT) MD								
LDA, fast cooling of l-Si (different steps) to 300 K, result for slowest cooling N,V,T with linear $V(T)$ to reproduce experimental densities of l-Si (melting point) and c-Si (300 K), subsequent annealing cycle for a-Si [111]			4.03	108.32	15.5	0.28		
GGA, fast cooling (2000 K/ps) of l-Si to 300 K N,V,T with V from the density of c-Si at 300 K, subsequent annealing cycle for a-Si [112]			3.96	107.38	15.2			
LDA, fast cooling of l-Si (different steps) to 0 K N,V,T with V from the density of c-Si at 300 K, subsequent annealing cycle for a-Si [113]			3.9			0.25		
Combined methods								

T3 potential, fast cooling of l-Si to 0 K and subsequent annealing steps, the last one at 1600 K with								
N,P,T with $P=0$		-1.6	4.05		11.7	0.19		
final DFT (GGA) relaxation to ground state, [114]		-3.3	4.01		9.7	0.14		
T3 potential, fast cooling of l-Si to 10 K, relaxation at $P=0$, annealing steps using DFT-MD, and relaxation to ground state (density equal to that of c-Si),			4.03	108.4		0.167		
further optimization by removing defects (atoms with high energy) [115]		-1.0	3.99-4.02	108.2	10.5	0.149		
SW-type potential of Vink *et al.* [103] , fast cooling of liquid-type Si to 300 K								
N,V,T with V from the experimental density of a-Si at 300 K [88]								
relaxation to ground state,			4.0	109.18	9.62		1.91	
additional relaxation by DFT (GGA) [116]			4.0	109.19	9.49			

Table IV. Activation enthalpy H_{act} and pre-factor v_0 of the SPER velocity: Simulation results for the different interatomic potentials and experimental data [7,11].

	H_{act} (eV)	v_0 (nm/ns)
SW, λ_0 [80]	1.44	3.40×10^5
SW, $1.3\lambda_0$	2.03	1.11×10^4
SW, $1.5\lambda_0$	2.16	6.60×10^3
T, T3 [35]	2.17	3.59×10^6
T, KMOD [105]	1.08	1.38×10^4
Ref. 7	*2.75*	*3.68×10^6*
Ref. 11	*2.70*	*4.64×10^6*

Table V. Total SPER simulation time (in ns) at respective temperatures. In several cases up to four simulations were carried out, which differ concerning the chosen initial heating rate and the coupling to the thermostat. The small numbers at high temperature indicate that full recrystallization occurs relatively fast.

T (K)	SW λ_0	SW $1.3\lambda_0$	SW $1.5\lambda_0$	T T3	T KMOD
800.	250				80, 70, 80, 70
850	150				60, 60, 60, 60
900	65, 65				40, 40, 40, 40
950	45, 50				20, 20, 20, 20
1000	35, 35				6, 6, 6, 6
1050	25, 25				
1100	12, 12				6, 6, 6, 6
1150	6, 6				
1200		2500, 3450, 2800, 3400		140	3, 6
1250		2050, 2400, 1800, 2400			
1300		750, 1200, 750, 1200		86	
1350		1050, 1200, 1050, 1200	2250, 2250		
1400		400, 400	1400, 1400	12	
1450		350, 350	1200, 1200		
1500		250, 250	400, 450	12	
1600		200, 200	300, 300	3	
1700		50, 50	150, 150	3	
1800			50, 50	3	
1900		50, 50	50,50	3	
2000		50, 50	50,50	1	

Table VI. Activation enthalpy H_{act} and pre-factor D_0 of the SD coefficient: Simulation results for the different interatomic potentials and experimental data [6].

	H_{act} (eV)	D_0 (cm^2/s)
SW, λ_0 [80]	1.53	7.77x10^{-2}
SW, $1.3\lambda_0$	2.02	8.35x10^{-4}
SW, $1.4\lambda_0$	2.09	3.70x10^{-4}
SW, $1.5\lambda_0$	2.28	6.36x10^{-4}
SW, Vink [103]	1.83	1.63x10^{-3}
SW, Albenze [104]	1.37	8.73x10^{-3}
T, T3 [35]	2.77	4.73x10^{1}
T, KMOD [105]	0.92	7.08x10^{-5}
Ref. 6	*2.70*	*5.50x10^{-2}*

Table VII. Total SD simulation time (in ns). The representation is similar to that in Table V.

T (K)	SW λ_0	SW $1.3\lambda_0$	SW $1.4\lambda_0$	SW $1.5\lambda_0$	SW Albenze	SW Vink	T T3	T KMOD
750								250
800	140, 800, 140, 800, 800, 800				400			100
850	400, 800, 300				300			100
900	360, 400, 400				200			100
950	360, 300				100			
1000	180, 300	3200, 3200	11300, 15350		100			100
1050	200, 90	2400, 2400	10800, 16400					100
1100	35, 35	1600, 1600	9300, 15350		40	1000		
1150	35, 35	1200, 1200	7800, 10900					100
1200		300, 1200	6400, 8000			800	250	
1250		220, 220, 800	5340					
1300		180, 180, 400	2280	1500, 1000, 1520		190	30	
1350		140, 400	2140	900, 1200, 1400				
1400		400, 400	1240	640, 600, 600			40	
1450		210		440, 600, 600				
1500		40, 210	340	320, 320, 320		90	30	
1600		20, 210	240	220, 220, 220		90	30 30	
1700		20,210	210	220, 220, 220			10	
1800		20,210	10	210, 200, 200			10	
1850				120				
1900		10		40			10	

2000		10, 10	10	10, 40			10	

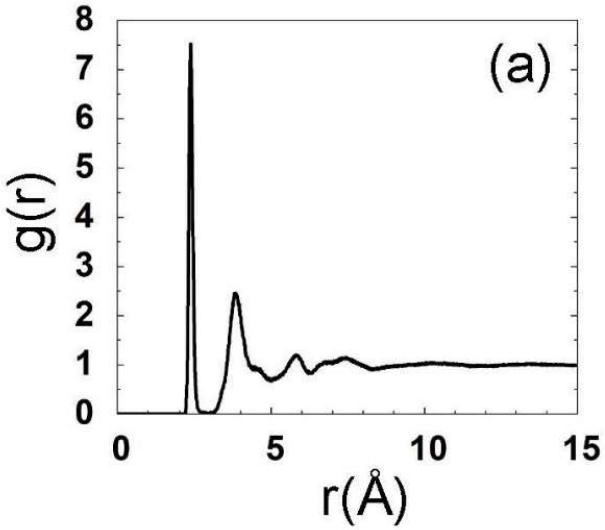
(a)
g(r)
r(Å)
0
1
2
3
4
5
6
7
8
0
5
10
15

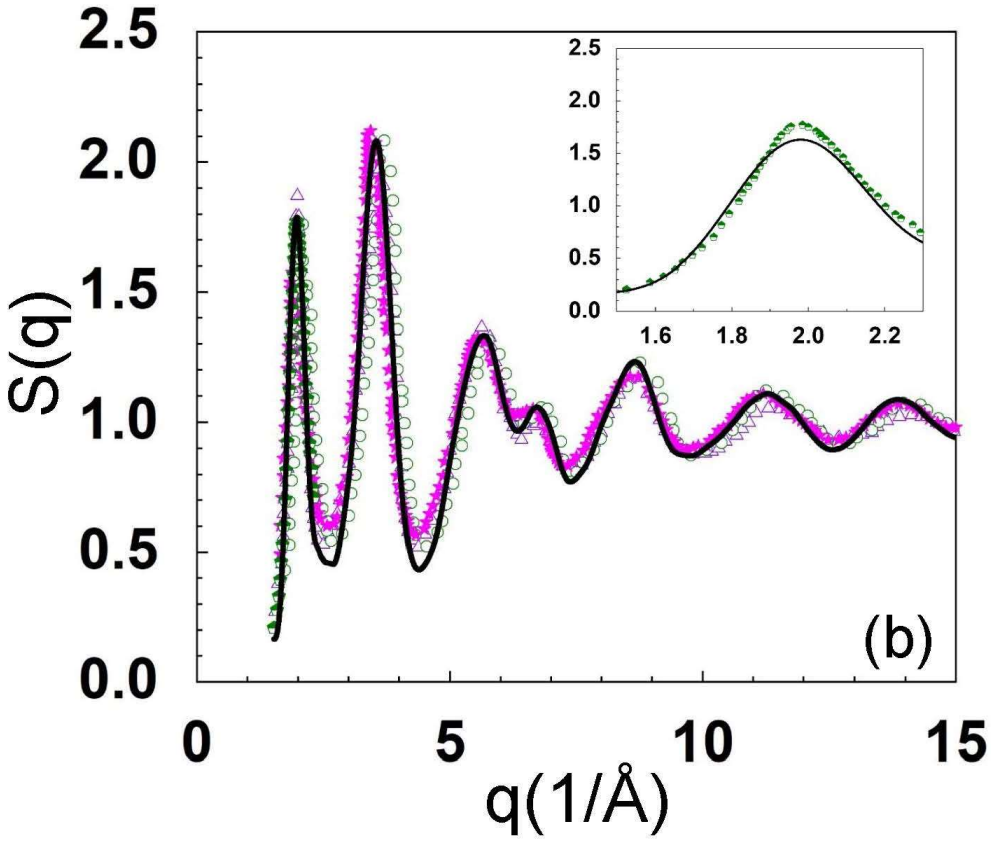
(b)
S(q)
q(1/Å)
0.0
0.5
1.0
1.5
2.0
2.5
0
5
10
15
1.6
1.8
2.0
2.2

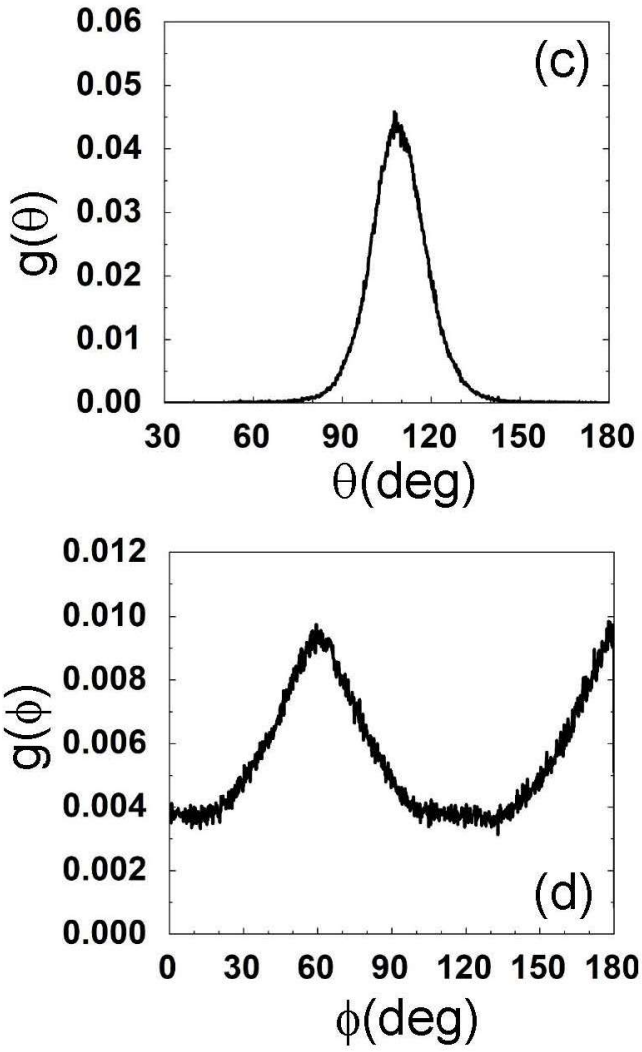

FIG. 1. Structural properties of a-Si at 300 K determined using the SW-type potential of Balamane *et al.* [80] (see Sec. III A 1): (a) pair correlation function, (b) static structure factor, (c) bond angle distribution, and (d) distribution of the dihedral angle. The symbols in (b) denote experimental data of Laaziri *et al.* [91] (olive open circles), Fortner *et al.* [92] (magenta stars), Kugler *et al.* [93] (open violet triangles), and Xie *et al.* [100] (olive triangles). The inset shows the latter data in more detail.

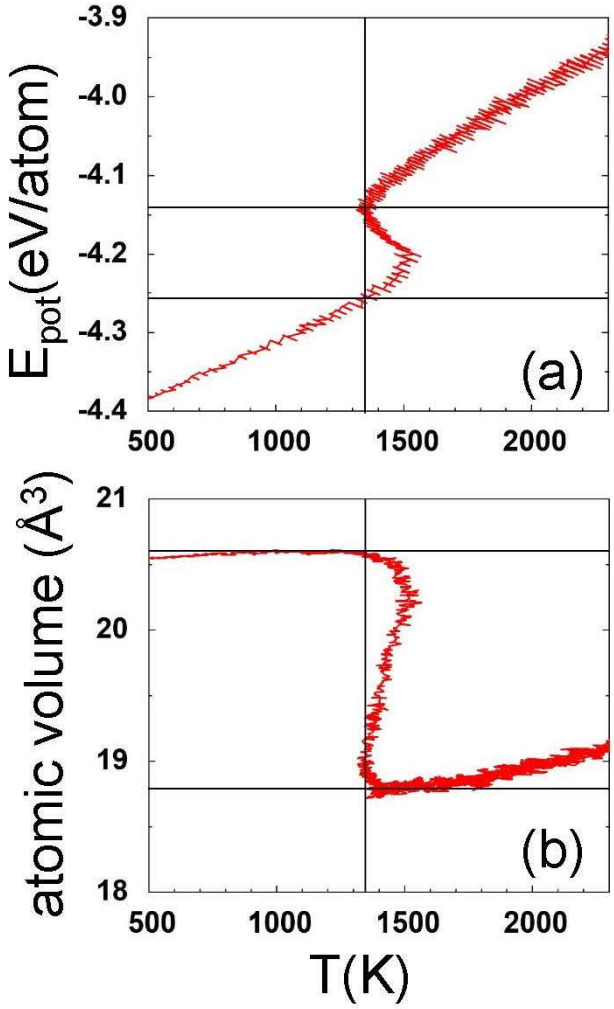

FIG. 2. Melting behavior of a-Si prepared using the SW-type potential of Balamane *et al.* [80] (see Sec. III A 1): (a) potential energy per atom in dependence on temperature and (b) atomic volume vs. temperature. The vertical line denotes the melting point.

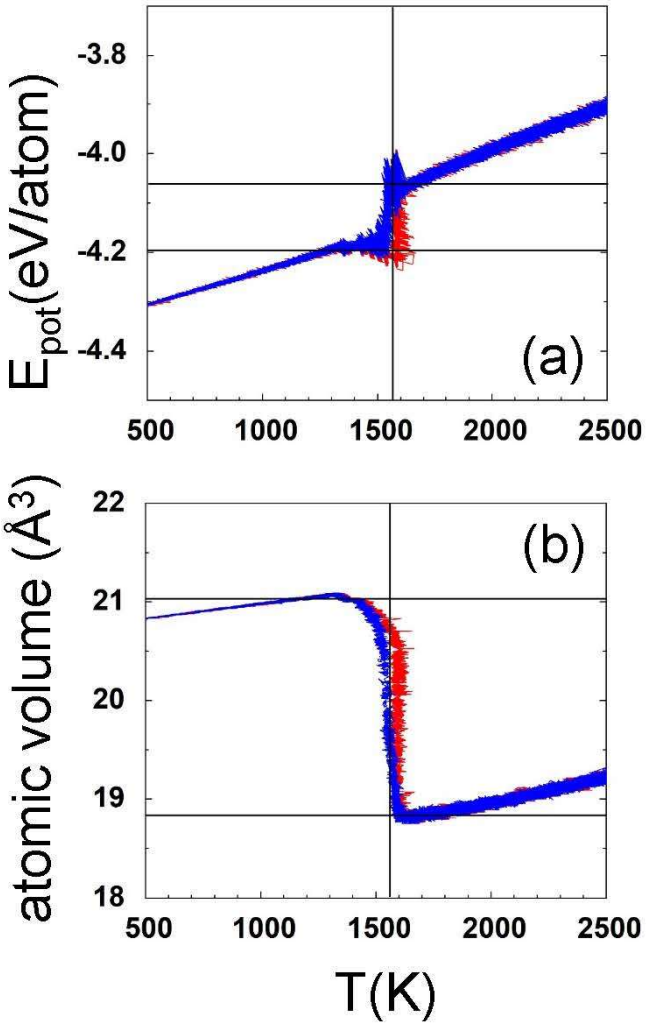

FIG. 3. Melting (red lines) and cooling (blue lines) behavior of the modified SW-type potential described in Sec. III A 4, Eq (1). For more details see caption of Fig. 2.

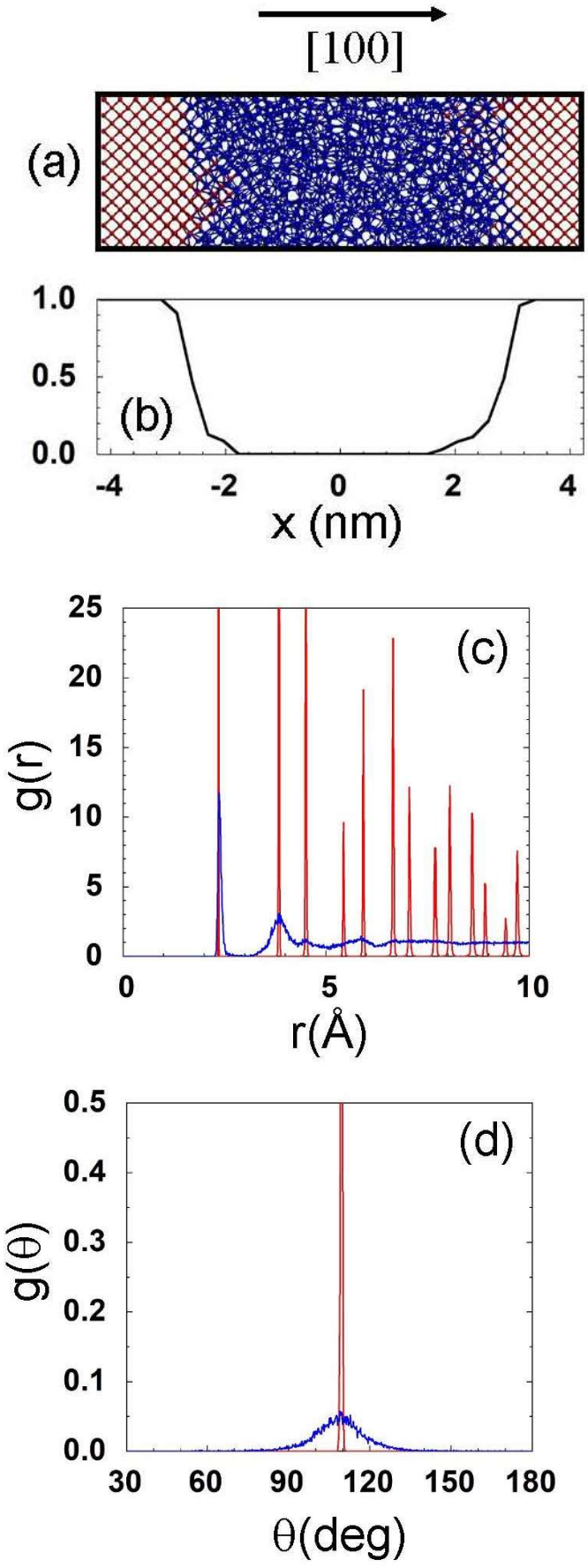
[100]
(a)
1.0
0.5
0.0
(b)
-4
-2
0
2
4
x (nm)
25
20
15
10
5
0
g(r)
(c)
0
5
10
r(Å)
0.5
0.4
0.3
0.2
0.1
0.0
g(θ)
(d)
30
60
90
120
150
180
θ(deg)

FIG. 4. Initial atomic configurations used in Sec. IV for the SPER simulation in the case of the SW-type potential of Balamane *et al.* [80]. The small spheres in (a) depict the positions of atoms time-averaged over 2 ps, at a temperature of 300 K. Atoms (and bonds) in the amorphous and the crystalline part are shown by blue and red color, respectively. The crystalline fraction in dependence on the x-coordinate is depicted in (b). For the time-averaged case the pair correlation function and the bond angle distributions for both the amorphous and crystalline part are presented in (c) and (d), respectively.

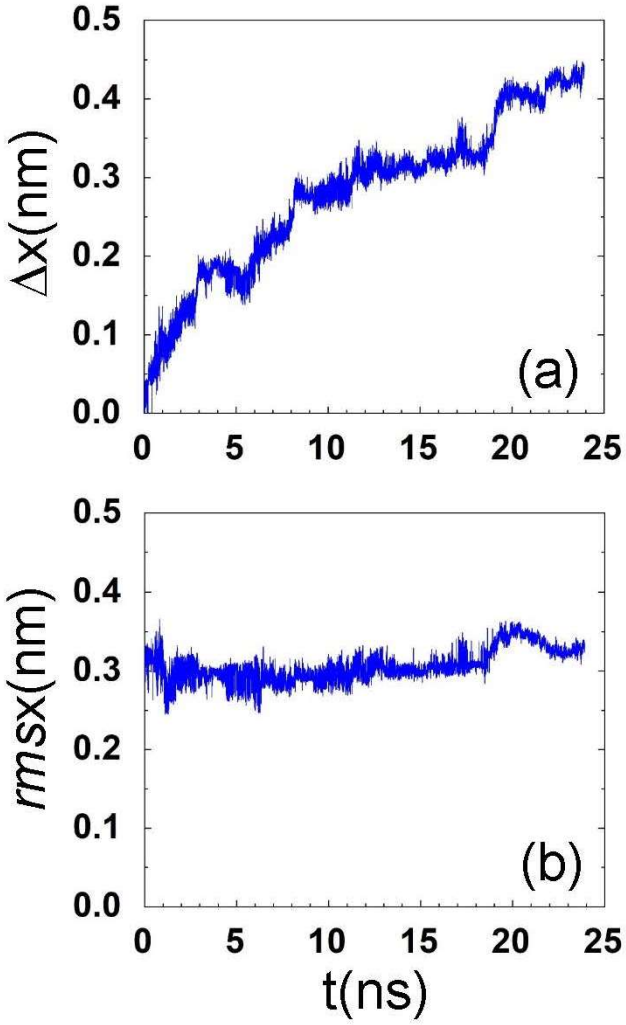

FIG. 5. Shift of the average position of the a-c interface with respect to the *x* axis versus time (a) and the time dependence of the *rms* deviation of this position (b). The data are shown for the example of SPER simulation at 1050 K using the same interatomic potential as in Fig. 4.

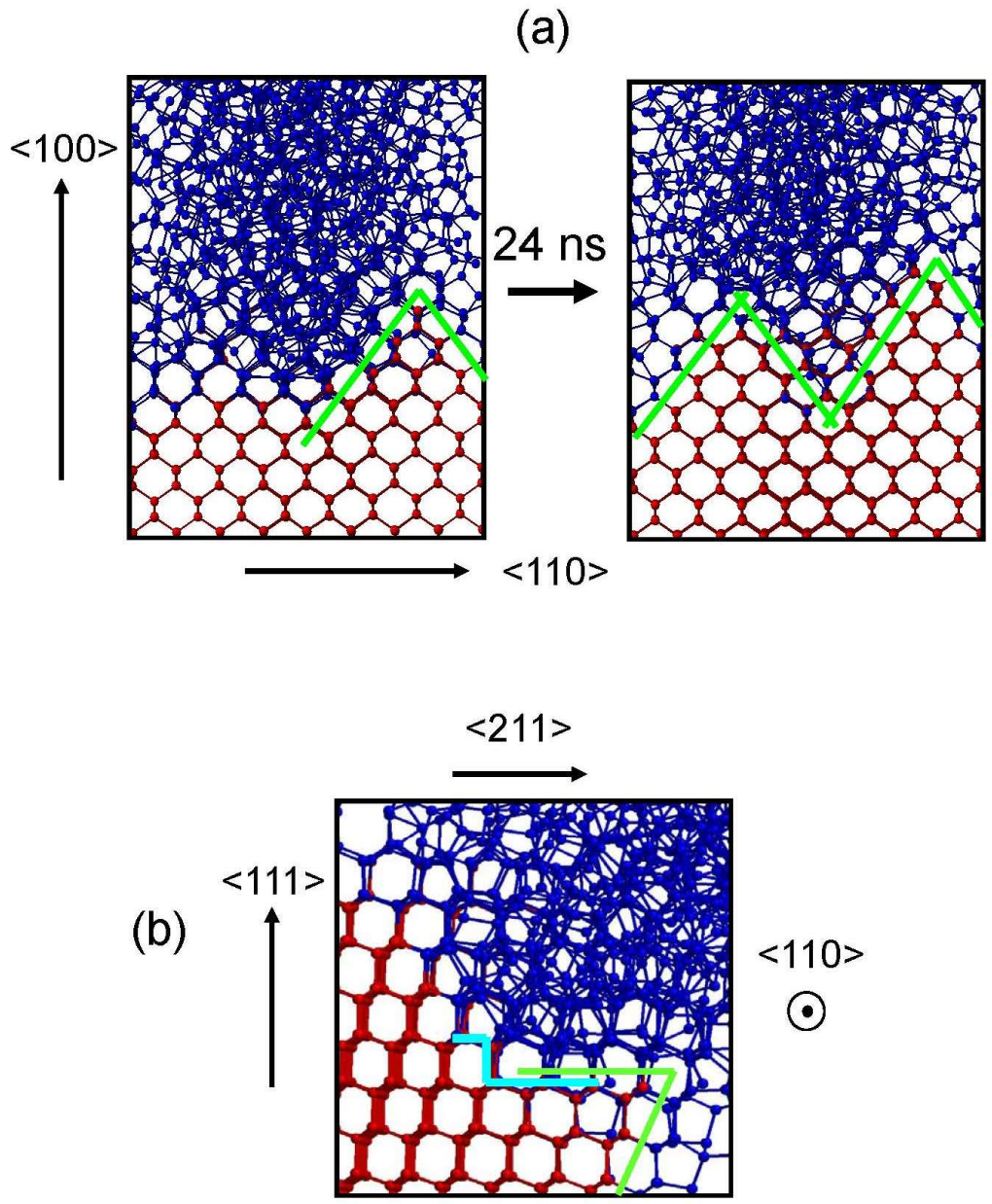

FIG. 6. Development of the a-c interface within 24 ns. The green lines mark the {111} facets or terraces where the sequential local rearrangement of atomic bonds occur. The picture is shown for the example of SPER simulation at 1050 K using the same interatomic potential as in Figs. 4 and 5. Figure (b) shows the projection of the left picture of figure (a) onto the {110} plane where the {111} terrace is also marked by cyan color.

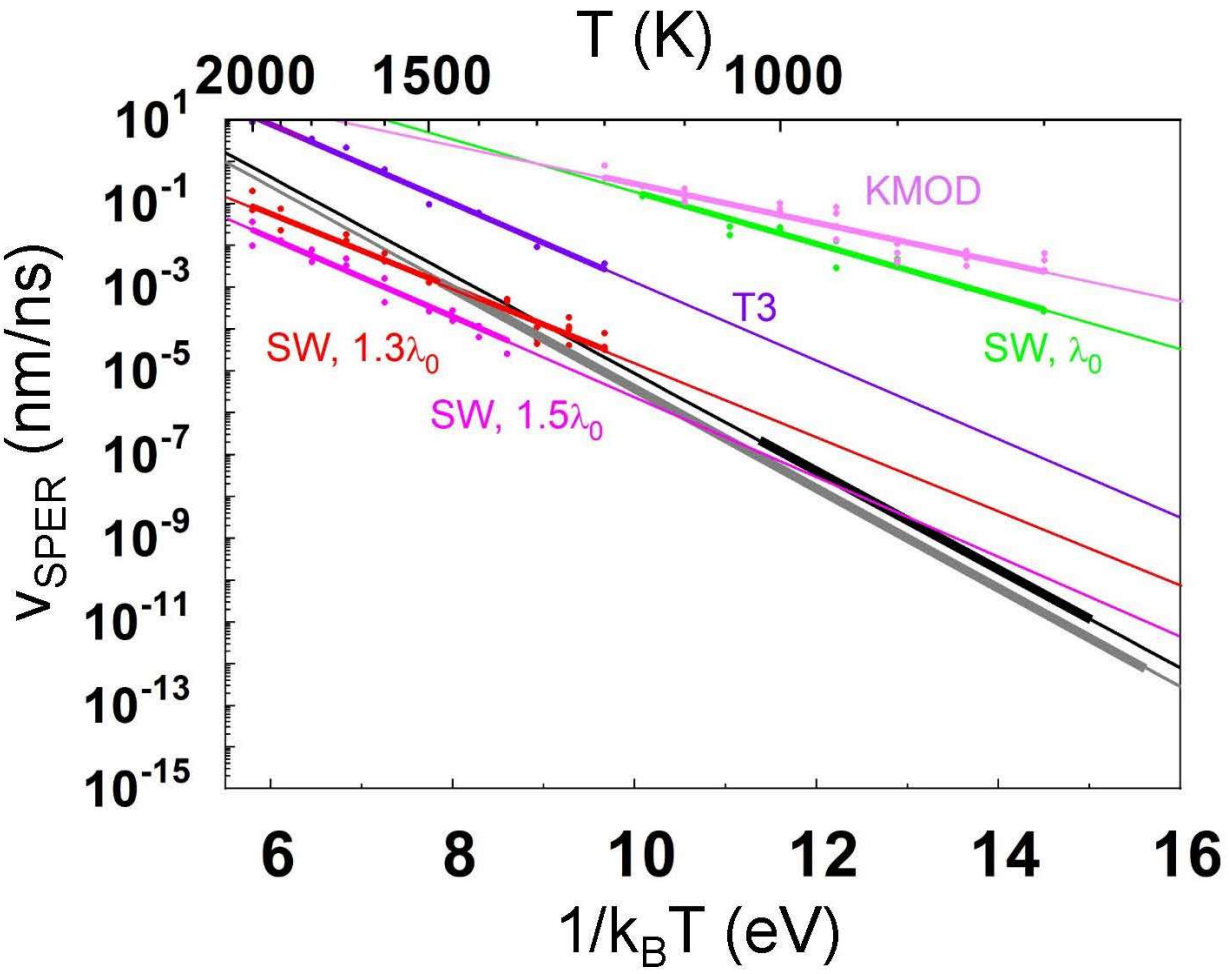

FIG. 7. SPER velocity obtained by MD simulations using different interatomic potentials. The data were determined for three versions of the SW-type potential of Balamane *et al.* [80] (see Sec. III A 1) which differ by the value of the three-body parameter λ , as well as for T-type potentials of Tersoff [35] (T3, see Sec. III B 1) and Kumagai *et al.* [105] (KMOD, see Sec. III B 2). The small colored circles are the calculated data and the straight

colored lines were obtained by the Arrhenius fit. The values for activation enthalpy and pre-factor obtained by the fit are given in Table IV. The lines are thicker in the temperature range in which simulations were performed. Furthermore, the figure shows black and gray lines which are fits to the most reliable and comprehensive experimental data sets [7,11]. The line thickness is increased in the temperature range in which the measurements were carried out.

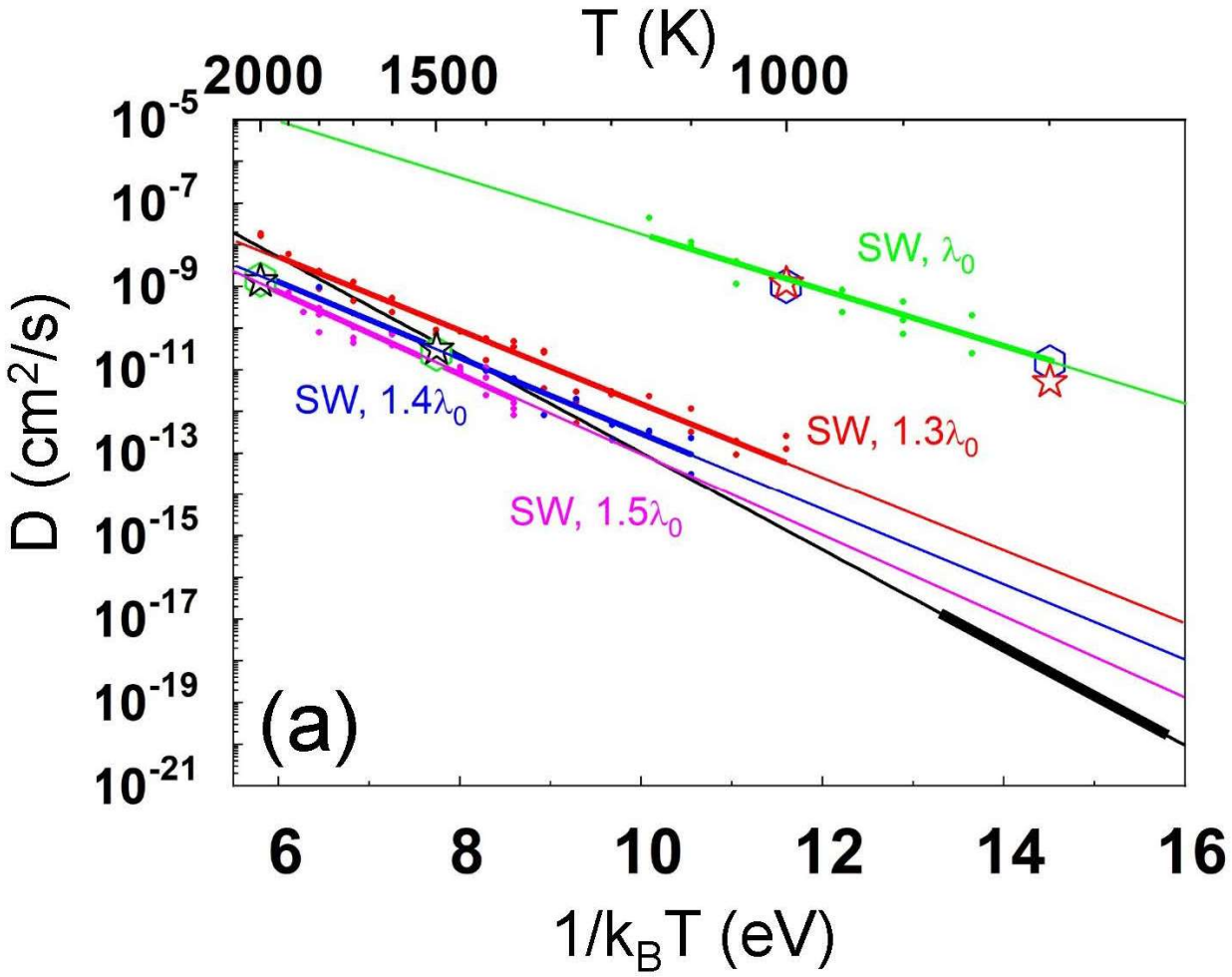
T (K)
2000
1500
1000
10^{-5}
10^{-7}
10^{-9}
10^{-11}
10^{-13}
10^{-15}
10^{-17}
10^{-19}
10^{-21}
D (cm^2/s)
SW, λ_0
SW, $1.4\lambda_0$
SW, $1.3\lambda_0$
SW, $1.5\lambda_0$
(a)
6
8
10
12
14
16
$1/k_BT$ (eV)

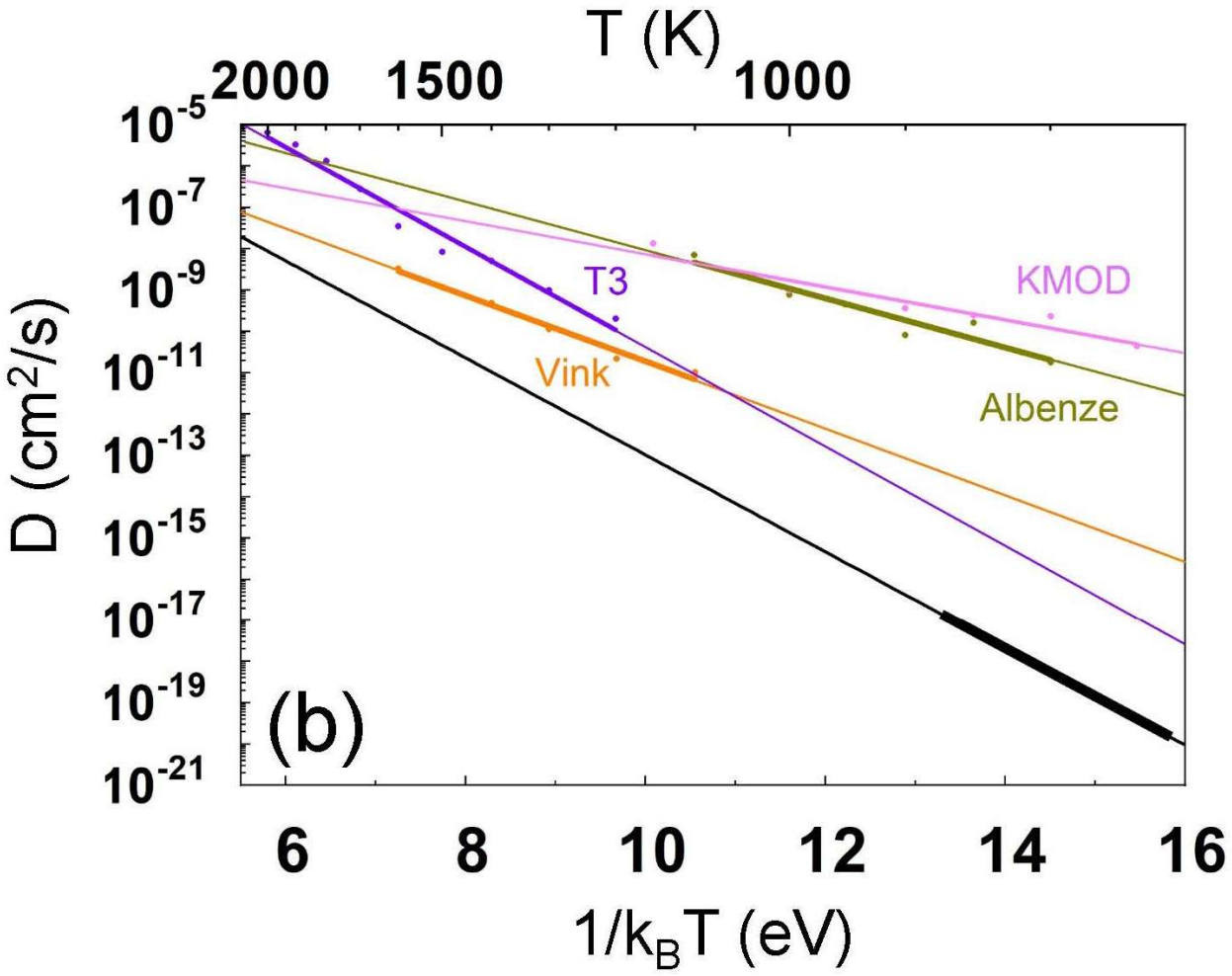

FIG. 8. SD coefficient of a-Si determined by MD simulations. The data of figure (a) were obtained by four versions of the SW-type potential of Balamane *et al.* [80] (see Sec. III A 1) with different values of the three-body parameter λ . Figure (b) depicts results calculated using the SW-type potentials of Vink *et al.* [103] (see Sec. III A 2) and Albenze *et al.* [104] (see Sec. III A 3) as well as the T-type potentials of Tersoff [35] (T3, see Sec.

III B 1) and Kumagai *et al.* [105] (KMOD, see Sec. III B 2). The scales on abscissa and ordinate and the color representation of the data are very close or identical to those in Fig. 7. Also, thick lines correspond to the temperature range where simulations and measurements were performed. The black line shows the fit to the experimental data of Ref. 6. In figure (a) the large hexagons and stars depict results of simulations with one vacancy or one self-interstitial in the MD cell, respectively.